Effects of congestion and confining walls on turbulent deflagrations in a hydrogen storage Facility-Part 2: Numerical Study

Vendra C. Madhav Rao[a], Pratap Sathiah[b] and Jennifer X. Wen[a,1]
[a]Warwick FIRE, School of Engineering, University of Warwick
Coventry, CV4 7AL, UK
[b]Shell Technology Centre Bangalore, Shell India Markets Private Limited, Plot No - 7, Bangalore Hardware Park, Devanahalli,Mahadeva Kodigehalli, Bangalore - 562 149, Karnataka, India

Abstract:
Safety studies for hydrogen retail stations involve identification of possible accidental scenarios, modelling of consequences and measures to mitigate associated hazards with it. Accidental release of hydrogen during its handling and storage can lead to formation of ignitable mixture in a very short time. Ignition of such a mixture can lead to generation of overpressure affecting structure and people. Understanding of the possible overpressures generated is critical in designing the system safe from explosion hazards. In the present study, the worst-case scenario where high-pressure hydrogen storage cylinders are enveloped by a premixed hydrogen-air cloud is numerically simulated. The computational domain mimics the setup for premixed hydrogen cloud in a mock hydrogen cylinder storage congestion environment experimentally studied by Shirvill et al. [1]. Large Eddy Simulations (LES) are performed using OpenFOAM CFD toolbox solver. The Flame Surface Wrinkling Model in LES context is used for modelling deflagrations [2]. Numerical simulation results are compared against experiments. Simulations are able to predict experimental flame arrival and overpressure reasonably well. The effects of ignition location, congestion and confining walls on the turbulent deflagrations in particular on explosion overpressure are discussed. It was concluded that explosion overpressure increases with increase in confinement.

Keywords: Hydrogen, Turbulent deflagration, Storage facility, Large Eddy Simulation, Flame Surface Wrinkling Model.

1. Introduction

Hydrogen energy is seen as the most likely future energy carrier to combat the adverse effects of climate change and depleting fossil fuels. One of the major potential applications of hydrogen is in hydrogen fuel cell vehicles. Handling and storage of hydrogen fuel is different from the convention fuels, due to its properties. Hydrogen is lightest of all gases, colorless, odorless, negative Joule-Thomson coefficient and highly flammable over wide range of hydrogen concentration (4-75–%). –Accidental release of hydrogen during its handling and storage can lead to formation of ignitable mixture in a very short time [3]. If this release is in an open area it will result in a flammable cloud. If it finds an ignition source, the result will be a cloud fire that burns back leaving a jet fire burning from the leak, until the supply is controlled or exhausted. If, however the jet release is into a confined or congested area an explosion may occur if the cloud is ignited. Depending on the type and degree of confinement or congestion, the explosion may result in an overpressure damaging to both equipment and people.

[1] Jennifer.wen@warwick.ac.uk

Understanding of the possible overpressures generated is critical in designing the system safe from explosion hazards. To address these issues, considerable amount of experimental and numerical work has been done in mock hydrogen refuelling and storage facility.

One such experimental study was performed by Shell Global Solution (UK) (in partnership with BP and Exxon Mobil) and HSL (UK). The study [4] was conducted in three parts. In the first part, a series of experiments were designed to establish hydrogen–air explosion overpressures in a well-defined, and well understood, repeated pipe congestion geometry. More realistic environments were chosen for the second and third parts. In the second part, experiments were performed to study the maximum overpressures generated in an ignited high pressure jet release and ignition of a premixed hydrogen-air cloud in a mock hydrogen refuelling station [5]. The effect of hydrogen concentration, ignition location and confining wall on generated explosion overpressures was studied. They found that the highest local overpressures were observed in the jet release experiments with a relatively short ignition time and concluded that two wall confinements give a more severe explosion than one wall confinement. In the third part a similar experiment was performed by [1]. The aim of the experiment was to study the maximum overpressure generated when hydrogen releases into array of dummy storage cylinders. The array of storage cylinders was used to represent high-pressure hydrogen cylinder storage congestion, and confining walls were used to represent isolation from the forecourt area. This experiment is basis of validation of numerical tool presented in this paper.

More detailed field tests were conducted by [6] on the dispersion and ignition of 40 MPa (400 barg) high-pressurized hydrogen gas releases to simulate the hypothetical scenario involving rupture of a pressurized pipe at a hydrogen refuelling station. The results indicated that the explosion overpressure was strongly dependent on the turbulent flow developed after the leakage of pressurised hydrogen. A similar experimental study was carried by [7] for hydrogen explosions overpressures in a model storage room, which is semi-confined in nature. It was found that the resulting overpressure varied significantly with hydrogen concentration. For hydrogen concentration (volume fraction) of up to 15 % the explosion overpressure generated was negligible, however for hydrogen concentration of 30 % whole of the model storage room experienced overpressures exceeding the tolerable limit. These experiments have provided useful insight to hydrogen explosion phenomena. Moreover, these experiments have also formed a useful database to aid the development and validation of CFD based numerical tools which can subsequently be used to design safe systems.

The numerical investigation was carried out using the commercial CFD code CFX [3] for the high pressure blowdown leak from hydrogen storage at 40 MPa based on experiments by [5]. The experiment represents an uncontrolled full bore failure of a vehicle refuelling hose, ignited using an electric spark. Pseudo diameter approach [3] was used to numerically simulate the high-pressure jet release and Turbulent Flame Closure model [8] was used to model the flame propagation. They concluded that the overpressures generated in a constant flow rate jet release case are higher than those generated in a blowdown jet release case. Numerical simulations [8] were performed for the hydrogen dispersion and combustion in an accidental scenario in a mock-up liquid hydrogen refuelling station, geometry setup based on experiments [5]. The effect of wind direction and ignition source on the dispersion and explosion overpressures of the hydrogen flammable cloud were investigated. CFD simulations were also performed [9,10] for premixed hydrogen air mixture explosion in a mock-up refuelling station based on experimental work of Shirvill et al. [5] by various researchers. Simulation results of various CFD models were compared against experiments. Results showed the prediction capabilities of various numerical and existing combustion models in use. The CFD models

Formatted: Indent: First line: 1.27 cm

have model constants and tuning parameters, which are difficult to determine apriori, hence validation of these CFD modelling along with the numeric is essential to ascertain their predictability.

The present paper reports numerical modelling of hydrogen explosion in a high-pressure hydrogen storage facility and comparison of results against the experiments reported in [1]. In the experimental campaign, one confining wall (High wall) and two confining wall (one high and one low wall) scenarios under different ignition locations were studied. The individual experiments were not repeated in the experimental campaign, mainly due to the associated prohibitive cost and difficulty in controlling the initial conditions in such large open air experiments. These experiments provided the information about the level of hazards and region of influence associated with hydrogen storage cylinders facility. There is a clear trend of higher overpressure magnitudes for explosions confined by high wall then the low wall. The use of high wall gives adequate protection to the personals in the vicinity of the facility but adversely increasing the explosion overpressure magnitudes. The two wall confinement are studied in experiments but the three wall confinements were not studied, which will considerably downsize the hazards zone. Thus as part of the numerical predictions these three wall scenarios are studied for two ignition locations, i.e. ignition near the high and low wall respectively. The effects of ignition location, congestion and confining walls on the turbulent deflagrations in particular on explosion overpressure are discussed. The experimental knowledge gap is supplemented by the numerical predictions.

The remaining paper is structured as follows.- The CFD and combustion model used is described in Section 2. In particular, the governing equations for combustion model (i.e. regress variable and flame surface density) and submodels for turbulent burning velocity and laminar burning velocity are presented. Section 3 and 4 describe the experimental setup and numerical settings used in our simulations. Section 5 presents results of the validation work. Finally, summary and conclusions are presented in Section 6.

Formatted: Normal

2. Mathematical modelling

The flow governing Navier-Stokes equations are solved using Large Eddy Simulation (LES) [12] method in OpenFOAM, which uses a collocated, finite-volume method, a fully compressible Pressure-Implicit Split Operator (PISO) solution method. Diffusion terms are discretized using a second-order accurate central differencing scheme and the advective terms approximated using a second-order accurate limited linear scheme. The transient term was discretized using a fully implicit, second-order accurate three-time-level method [13]. A one equation eddy viscosity model is used for evaluating the sub-grid scale turbulence [15]. The main difficulty in combustion LES is the proper treatment of the flame front or the reaction zone, since the characteristic scales for the reaction process are in the sub-grid scale, hence Subgrid-Scale (SGS) reaction rate models are required. The Flame Surface Wrinkling Model developed by [14] is adopted for simulating the turbulent deflagrations. The set of governing equations are solved sequentially with iteration over the explicit coupling terms to obtain convergence. A Courant number [13] of 0.1 was used in the present numerical simulations. The following section describes the combustion model used in the modelling work.

2.1Combustion Model

The laminar flamelet approach is used with conditional filtering to create a set of transport equations representing the complex combustion process [2,14]. The flamelet concept simplifies the turbulent combustion treatment by separating the combustion modelling from the analysis of the turbulent flow field by assuming that reaction takes place in relatively thin layers that

separate regions of unburned and fully burned gases. The unburnt zone volume fraction is denoted as regress variable (b), taking values $b = 1$ in fresh gases and $b = 0$ in fully burnt gas region. The transport equation for the resolved part of regress variable is given as:

$$\frac{\partial \bar{\rho}\tilde{b}}{\partial t} + \nabla.\left(\bar{\rho}\tilde{U}\tilde{b}\right) - \nabla.\left(\bar{\rho}\mu_{sgs}\nabla\tilde{b}\right) = -\bar{\rho}_u S_L \Xi \left|\nabla\tilde{b}\right| \quad (1)$$

where, Ξ is sub-grid flame wrinkling, can be regarded as the turbulent to laminar flame speed ratio and is formally related to the flame surface density by $\Sigma = \Xi |\nabla\bar{b}|$, ρ is the density, S_L is laminar flame speed and μ_{sgs} is the sub-grid turbulent diffusion coefficient. Symbols ($\bar{}$) and ($\tilde{}$) represent the filtered and the density weighted filtering operations, respectively. The subscripts u indicates conditioning on the unburned gases region. The resolved unburned gas volume fraction $\bar{b}$ is related to $\tilde{b}$ through $\bar{\rho}_u \bar{b} = \bar{\rho}\tilde{b}$. The closure for the sub-grid wrinkling is provided by a balanced transport equation,

$$\frac{\partial \bar{\rho}\Xi}{\partial t} + \hat{U}_s.\nabla\Xi = \bar{\rho}G\Xi - \bar{\rho}R(\Xi - 1) + \bar{\rho}\max\left[(\sigma_s - \sigma_t), 0\right]\Xi \quad (2)$$

where, $\hat{U}_s$ is the surface filtered local instantaneous velocity of the flame, which is modelled as

$$\hat{U}_s = \tilde{U} + \left(\frac{\bar{\rho}_u}{\bar{\rho}} - 1\right) S_L \Xi n_f - \frac{\nabla(\bar{\rho}\mu_{sgs}\nabla\tilde{b})}{\bar{\rho}|\nabla\tilde{b}|} n_f \quad (3)$$

The direction of flame propagation is $n_f = \nabla\tilde{b}/|\nabla\tilde{b}|$, σ_s and σ_t are the surface filtered resolved strain-rates relating to the surface filtered local instantaneous velocity of the flame ($\hat{U}_s$) and surface filtered effective flame velocity of the flame surface ($\hat{U}_t$), modelled as

$$\sigma_t = \nabla.(\tilde{U} + S_L \Xi n_f) - n_f.[\nabla(\tilde{U} + S_L \Xi n_f)].n_f$$

$$\sigma_s = \frac{\nabla.\tilde{U} - n_f.(\nabla\tilde{U}).n_f}{\Xi} + \frac{(\Xi + 1)[\nabla.(S_L n_f) - n_f.[\nabla(S_L n_f).n_f]}{2\Xi} \quad (4)$$

The terms $G\Xi$ and $R(\Xi - 1)$ in Eq. 2 are sub-grid turbulence generation and removal rate, with G and R as rate coefficients which requires further modelling. The modelling of these terms is based on flame-speed correlation of [16] are given below

$$G = R\frac{\Xi_{eq} - 1}{\Xi_{eq}} \quad \text{and} \quad R = \frac{0.28}{\tau_\eta}\frac{\Xi^*_{eq}}{\Xi^*_{eq} - 1},$$

$$\Xi^*_{eq} = 1 + 0.62\sqrt{\frac{\hat{u}}{S_{L\,\eta}}}\,R_\eta \quad \text{and} \quad \Xi_{eq} = 1 + 2(1 - \tilde{b})(\Xi^*_{eq} - 1) \quad (5)$$

where, τ_n is the Kolmogorov time scale, $\hat{u}$ is the sub grid turbulence intensity and $\mathcal{R}_\eta$ is the Kolmogorov Reynolds number.

The closure for the unstrained laminar speed is expressed as power law function of elevated temperature (T) and pressure (P) similar to the expression of [17],

$$S_L(\tilde{T}, \bar{P}) = S_{L,0}\left(\frac{\tilde{T}}{T_0}\right)^\alpha \left(\frac{\bar{P}}{P_0}\right)^\beta \quad (6)$$

The unstrained laminar burning velocity ($S_{L,0}$) correlation based on [18] work is been used for evaluating S_L at a given equivalence ratio (ϕ) and reference condition,

$$S_{L,0} = 2.1087\phi^5 - 8.6278\phi^4 + 10.455\phi^3 - 2.8908\phi^2 + 1.3031\phi - 0.1075 \text{ for } \phi < 1.7$$

$$S_{L,0} = 0.0027\phi^5 - 0.067\phi^4 + 0.645\phi^3 - 2.8799\phi^2 + 5.1941\phi - 0.1446 \text{ for } \phi > 1.7 \quad (7)$$

The above correlation is valid for equivalence ratios between 0.13 and 7.1 (flammability limits). The temperature and pressure exponents for hydrogen-air mixture are taken as α =1.4 and β = 0.194 respectively, with reference state as T_0 = 291 K, P_0 = 1 atm. The equation (1)-(6) completes the combustion model description. The closure for subgrid scale viscosity is provided using subgrid scale kinetic energy (k_{sgs}), computed by solving the one equation eddy viscosity model in OpenFOAM [13].
The sub-grid viscosity (μ_{sgs}) is modelled as

$$\mu_{sgs} = C_k \bar{\rho} k_{sgs}^{1/2} \bar{\Delta} \quad (8)$$

where, $\bar{\Delta} = (\Delta x \Delta y \Delta z)^{1/3}$ is characteristic length scale , $(\Delta x, \Delta y, \Delta z)$ are mesh size in x, y and z-coordinate directions) and $C_k = 0.094$ is model constant. A transport equation for subgrid kinetic energy is better suited for non-uniform grids and the also accounts for non-equilibrium effects within the source terms.

Formatted: Space Before: 6 pt, After: 6 pt

Field Code Changed

Field Code Changed

Field Code Changed

Field Code Changed

Field Code Changed

Field Code Changed

3. Experimental Setup

The overall length of cylinder was 2.64 m, diameter 0.80 m with one end fitted with an approximately 106˚ shroud extending 60 mm beyond the end of the cylinder. The cylinder storage congestion rig was constructed by HSL and comprised a lifting frame containing two rows of five cylinders. Further details of this are available in part-1 [1] of the experimental facility paper.

(a)

(b)

Figure 1. Experimantal setup for (a) one confining wall and (b) two confining walls.

The cylinder rig was confined by one or two walls, 4.8 m and 2.5 m high. Furthermore, the cylinder rig was placed 1 m from a 4.8 m high and 5.4 m long wall (referred as high wall). It was surrounded by a 5.4 x 6.0 x 2.5 m frame (made from 25 mm square hollow section steel) to hold the premixed hydrogen-air mixture. The sides of the frame and the outside of the wall(s) were covered with a thin (23 μm) plastic film, similar to cling film. The film was held to the sides of the frame by using spray-on contact adhesive. The plastic film was not cut along the sides before the trials. For two confining wall trials, an additional 2.5 m high 6.0 m long wall (referred as low wall) was used to provide more confinement. The cylinder congestion rig with confining walls and the plastic film in position is shown in Figure 1(a) and (b) for one and two walls experiments, respectively.

~~The overall volume of hydrogen-air contained within the storage rig was 67.59 m^3 with corresponding volume blockage of 16.56 %. Hydrogen cylinder storage congestion with two different ignition locations and different confining walls is considered in the present study for the validation work. In Table 1, the basic details of each case considered in present study are been summarized. A schematic representation of test facility is available in Fig. 2 (a). The locations of the overpressure monitoring points are shown in elevation and plan view in Figures 2(b) and (c), respectively. Figure 2(c) also shows different ignition location P1 and P4 for different experiments used for numerical validation.~~

Table 1. Premixed hydrogen-air experimental and numerical conditions.

Parameter	**CASE-A** ~~**(h2cyl06)**~~	**CASE-B** ~~**(h2cyl11)**~~	**CASE-C** ~~**(h2cyl12)**~~	**CASE-D**	**CASE-E**
Cases	~~Expt~~Experiment (h2cyl06)~~.~~	Experiment (h2cyl11)~~t.~~	Experiment (h2cyl12)~~.~~	Numerical simulation~~s~~	Numerical simulation~~s~~
No. of walls	1	2	2	3	3
Free volume (m^3)	67.59	67.59	67.59	67.59	67.59
Ignition position (m)	P1 (High Wall) (0.59, 2.74, 1.24)*	P4 (Low Wall) (3.30, 0.75, 1.24)	P1 (High Wall) (0.59, 2.74, 1.24)	P4 (Low Wall) (3.30, 0.75, 1.24)	P1 (High Wall) (0.59, 2.74, 1.24)

Formatted: Font: Bold
Formatted: Space Before: 6 pt, After: 6 pt
Formatted Table
Formatted: Space After: 6 pt
Formatted: Space After: 6 pt
Formatted: Space Before: 6 pt, After: 6 pt
Formatted: Space After: 6 pt
Formatted: Font: 11 pt
Formatted: Font: 11 pt
Formatted: Font: 11 pt
Formatted: Font: 11 pt
Formatted: Font: 11 pt
Formatted: Space After: 3 pt
Formatted: Font: 8 pt
Formatted: Font: 8 pt
Formatted: Font: 8 pt
Formatted: Font: 8 pt
Formatted: Font: 8 pt

Gas mixture temperature (˚C)	19.4	19.4	31.7	31.7	31.7
Mass of hydrogen (kg)	1.77	1.96	1.94	1.94	1.94
Stoichiometric ratio of mixture	1.1	1.22	1.27	1.27	1.27
Computational domain size (m^3)	25 x 27 x 12	25 x 25 x 12	~~25~~ 25x 25 x 12	~~26~~ 25 x 20 x 12	~~27~~ 25 x 20 x 12

*(0,0,0) origin coordinate is at corner of concrete block walls.

The overall volume of hydrogen-air contained within the storage rig was 67.59 m^3 with corresponding volume blockage of 16.56 %. Hydrogen cylinder storage congestion with two different ignition locations and different confining walls is considered in the present study for the validation work. In Table 1, the basic details of each case considered in present study are been summarized. A schematic representation of test facility is available in Fig. 2 (a). The locations of the overpressure monitoring points are shown in elevation and plan view in Figures 2(b) and (c), respectively. Figure 2(c) also shows different ignition location P1 and P4 for different experiments used for numerical validation.

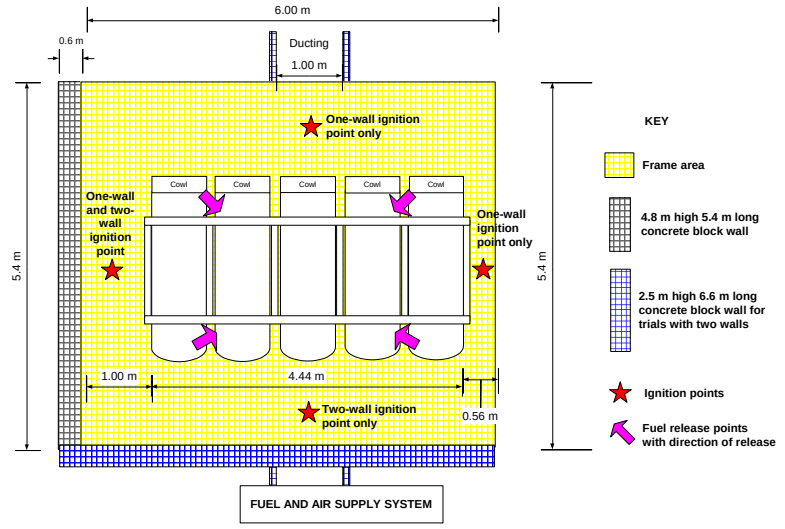

(a) Premixed cloud layout

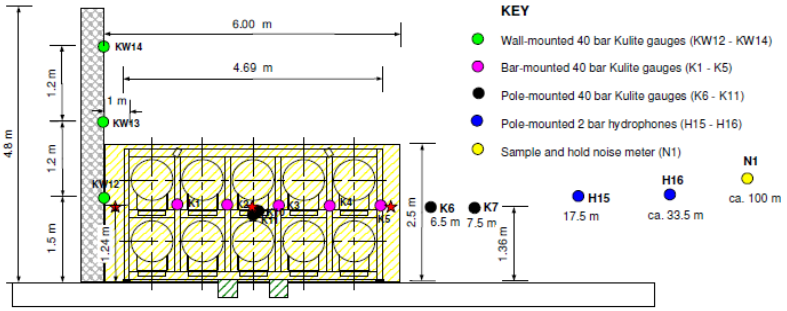

(b) Elevation view

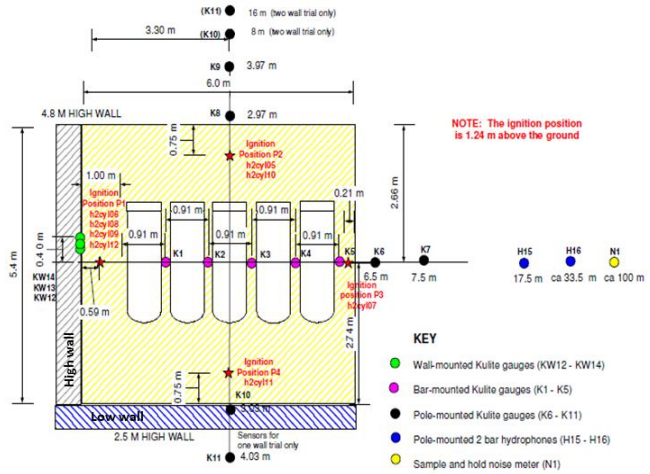

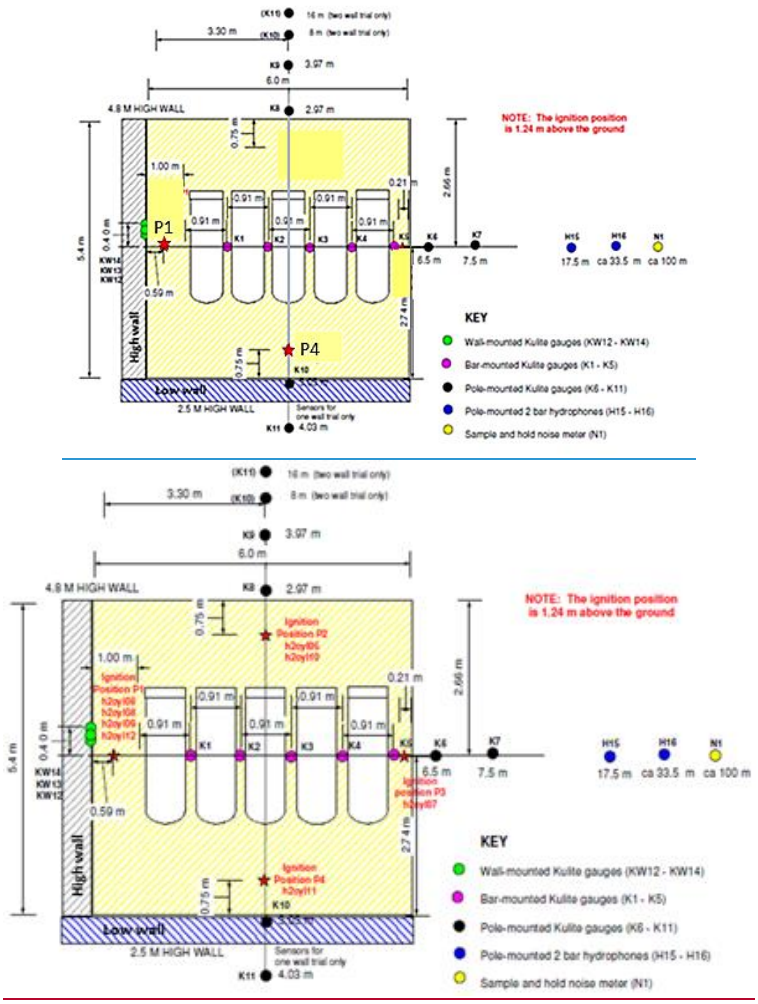

(c) Plan view

Figure 2~~(a)~~ Schematic representation of test facility and experimental pressure (sensors) monitoring point locations ~~(b) (elevation view)~~[1] ~~and (c) (plan view)~~[1].

4. Numerical setup

The experiments and numerical simulations mentioned in the Table 1 are here after referred as CASE-A, CASE-B, CASE-C, CASE-D and CASE-E, respectively. The computational ~~domain~~ geometry for different confining wall scenarios is shown in Figure ~~5~~ 3 (x-y plane is the ground

Formatted: Centered

level and the z-direction is the elevation). ~~The dimensions of t~~The simulation domain extends were chosen large enough s~~uch~~ that the effects of end boundary condition were minimal on the predictions at the monitoring locations close to the rig as given in Table 1. The cylinder ends are modelled without shroud ~~extending~~extensions, to reduce the meshing complexity. The premixed near stoichiometric hydrogen-air cloud is initialized using 'setField' utility in OpenFOAM (further details are available in [13]). This is shown as the ~~dark~~ shaded colored region in Figure ~~6~~4. The ambient conditions are taken as 1 atm pressure with no wind conditions. Further simulation parameters are ~~defined~~ presented ~~(~~in Table 1~~1) with no wind conditions~~. Ignition of the premixed cloud is initiated with an ad-hoc spark ignition model for regress variable in OpenFOAM, located close to either High or Low wall at 1.24 m above the ground ~~as~~ (mentioned in Table 1). For the numerical simulations with three confining walls, i.e., one High wall and two Low walls are considered as shown in Figure 5(c). It is worth noting that first three cases in Table 1 corresponds to validation of OpenFOAM CFD code, and last two cases in Table 1 corresponds to pure numerical investigation. Cases-D and Case-E corresponds to case where effects of increase in overpressure due to increase in confinement by adding an extra wall is investigated.

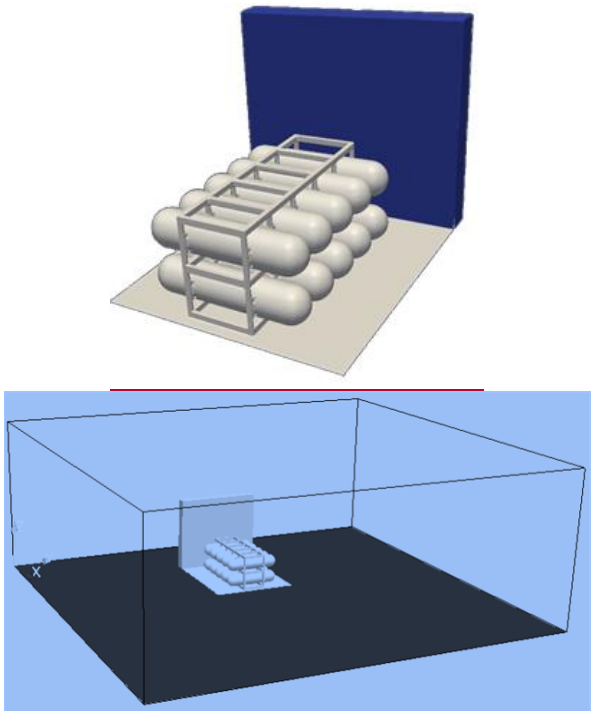

(a) One wall high wall - (CASE-A)

Formatted: Centered

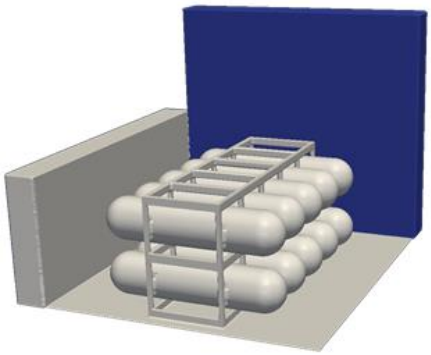

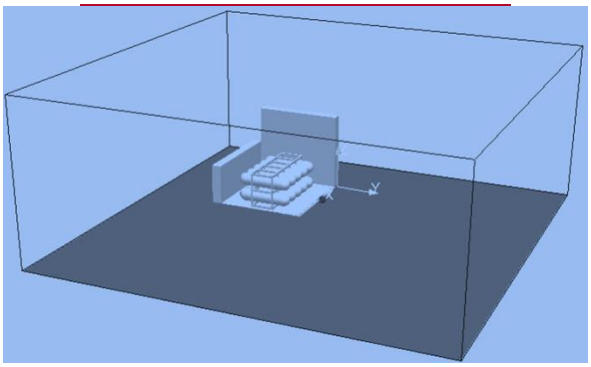

(b) ~~Two wall~~One high wall and one Low ~~wall~~ (~~wall~~ (CASE-B & C)

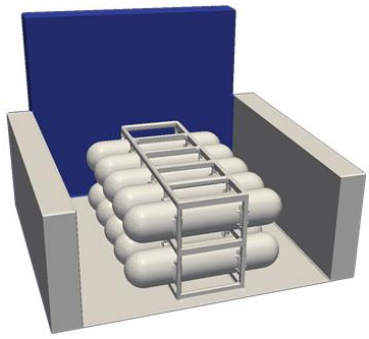

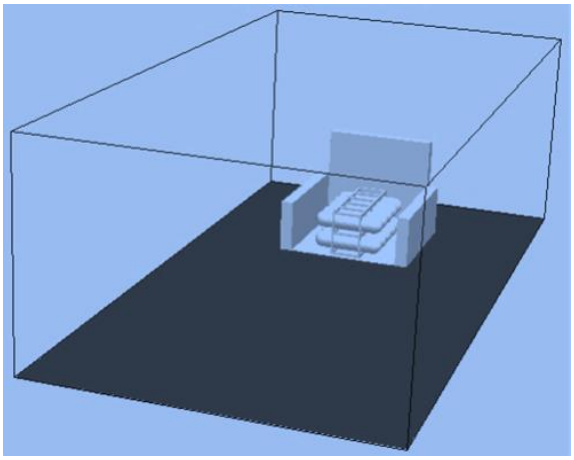

(c) One high wall and two low walls ~~Three wall~~ (CASE-D & E)

Figure ~~5~~3. Computational domain showing wall boundaries

No-slip and adiabatic boundary condition are imposed on the wall surfaces. Improper treatment of pressure and velocity at outlet boundary in simulations can lead to spurious numerical wave reflections that can seriously affect the solution. A partial non-reflective pressure boundary condition is implemented in OpenFOAM named as 'waveTransmissive' is applied to pressure and 'zeroGradient' condition is applied for the velocity at the domain enclosure surface (outlet). Further details of the boundary condition are available in [13]. The initial turbulence in the computational domain was set using random number generator for a homogenous resolved velocity fluctuation of 0.12 m/s.

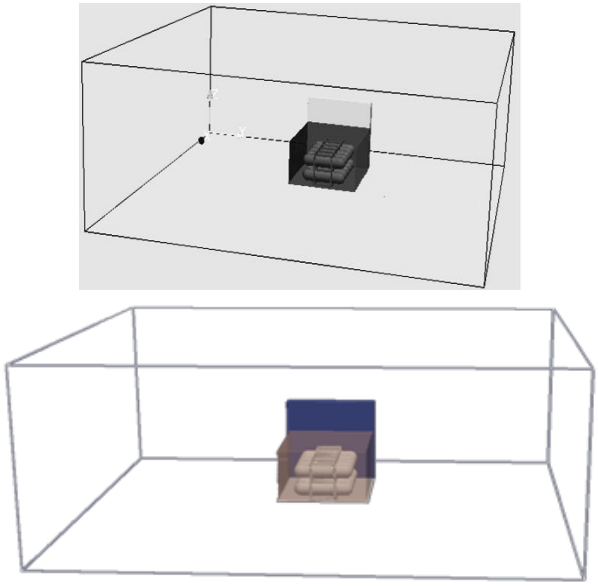

(a) With one High wall

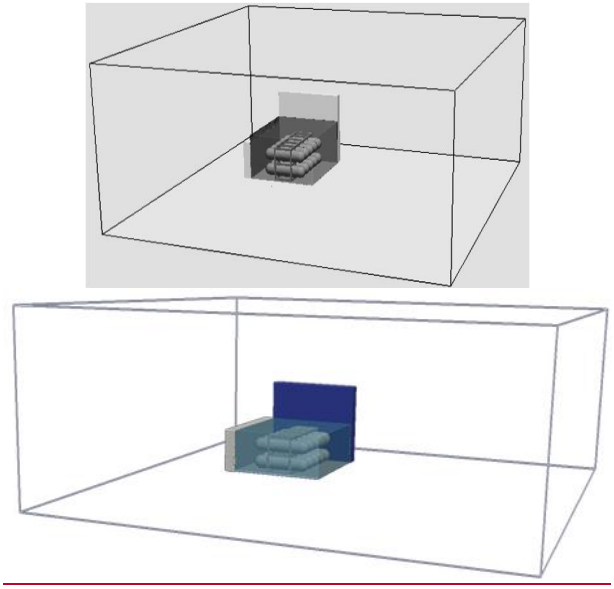

(b) With one ~~H~~high and one ~~L~~low wall

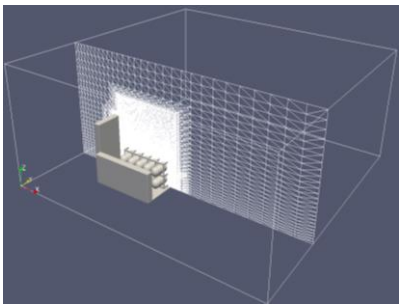

(~~a~~c) Vertical plane

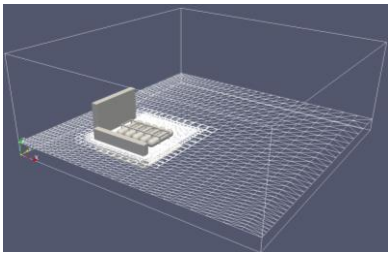

(d~~b~~) Horizontal plane

Figure ~~6~~ 4 (a) and (b) Premixed vapour cloud initialization (~~dark~~ shaded region). (c) and (d) corresponds to mesh distribution in the plane of ignition location.

Table 2. Overpressure Monitoring point location (*present for one wall simulation only, Figure 5(a)). Figure 3(b) and 4 provides location of different probes.

Monitoring point No.	Height above ground (m)	Distance from High wall (m)
K1	1.36	1.91
K2	1.36	2.82
K3	1.36	3.73
K4	1.36	4.64
K5	1.36	5.55
K6	1.36	6.5
K7	1.36	7.5
	Height above the ground	Distance from Rig centre
K8	1.36	2.97
K9	1.36	3.97
K10	1.36	3.03*
K11	1.36	4.03*
	Distance up the High wall	Distance from Rig centre
KW12	1.5	0.4
KW13	2.7	0.4
KW14	3.9	0.4

Formatted: Centered

Formatted Table

The computational domain is discretized into non-uniform hybrid mesh (mix of hex. and tet. cells) using 'snappyHexMesh' utility with in the OpenFOAM. The key parameters in snappyHexMesh utility that were adjusted to get an appropriate mesh were the surface and 'search region' refinement levels, which were set to minimum and maximum levels of 4 & 6 and 3 & 5 respectively. The search region was specified with dimensions of 7 x 7 x 10 m^3, as shown in Figure 4(c) & (d) with refined mesh. ~~A representative mesh distribution for the two-wall scenario is shown in Figure 7, the mesh size varied from 5 mm at the ignition location to 60 cm at the domain boundary. The mesh is further refined towards the cylinder and frame solid surfaces, to adequately capture the flame propagation with in the congestion.~~There is also a control parameter in 'snappyHexMesh' to restrict the overall mesh size to a given limit. A representative mesh distribution for the two-wall scenario is shown in Figure ~~7~~4, the mesh size varies from 5 mm at the ignition location to 60 cm at the domain boundary. Within the region of flame propagation, the average mesh size is around 8mm. The mesh is further refined into layers towards the cylinder and frame solid surfaces, to adequately capture the flame propagation with~~–~~in and near the congestions. ~~–in the region of interest for the flame propagation.~~

Formatted: Justified

The respective ~~CASEs~~ CASE's (A-E) are discretized into 5 to 6.5 million finite volume cells. The typical computation time for one simulation was around 32 hours using 80 cores with average time step in the order of 10^{-6} s for the temporal numerical integration. The probe data is recorded after every five time-step iterations during the simulations. The location for pressure probes monitoring the overpressures in a simulation are listed in Table 2. The monitoring points K1 to K5 are inside the congestion (rig) and within the premixed vapour cloud. K6 and K7 are outside the vapour cloud and 1 m apart in direction away from the High wall. Locations K8 and K9 / (K10 and K11) are 1 m apart, also lie outside the vapour cloud in parallel direction to the High wall as shown in Figures ~~3 and 4~~2 in elevated and plan views.

The ignition model parameters: Ignition diameters, ignition duration, strength of ignition, ignition lag and velocity fluctuations were initially adjusted to match the initial pressure rise profile for the Case-A, then they were left unchanged for the remaining simulations.

5. Results and discussion

In this section, flame arrival time and pressure profile as a function of time measured at different probes are compared against experimental results for CASE-A to C. Numerical investigations are presented for the CASE-D and CASE-E.

5.1 CASE–A: One wall scenario (High wall ignition)- CFD model validation

Flame and pressure dynamics obtained using simulations are compared against experiments for CASE-A in this section.

Formatted: Indent: Left: 0 cm

Figure ~~7~~ 5 shows the contours and iso-surfaces of regress variable, *b* at different time instants. Top figure shows the contours on a vertical plane and bottom figure shows the contours on a

horizontal plane. Figure in the middle shows iso-surface of regress variable corresponding to regress variable of *b*=0.5. Since ignition in this case was ~~too~~ close to the high wall, flame surface starts to develop close to the high wall. ~~As the flame front propagates, the unburnt gas ahead of the flame is pushed through the cylinders leading to enhancement of turbulence which results in increase in flame speed. This increase in flame speed results in elongation of the leading edge of the flame surface (see top figure (a) to (e)). The trailing edge of the flame slowly moves along the length of high wall.~~

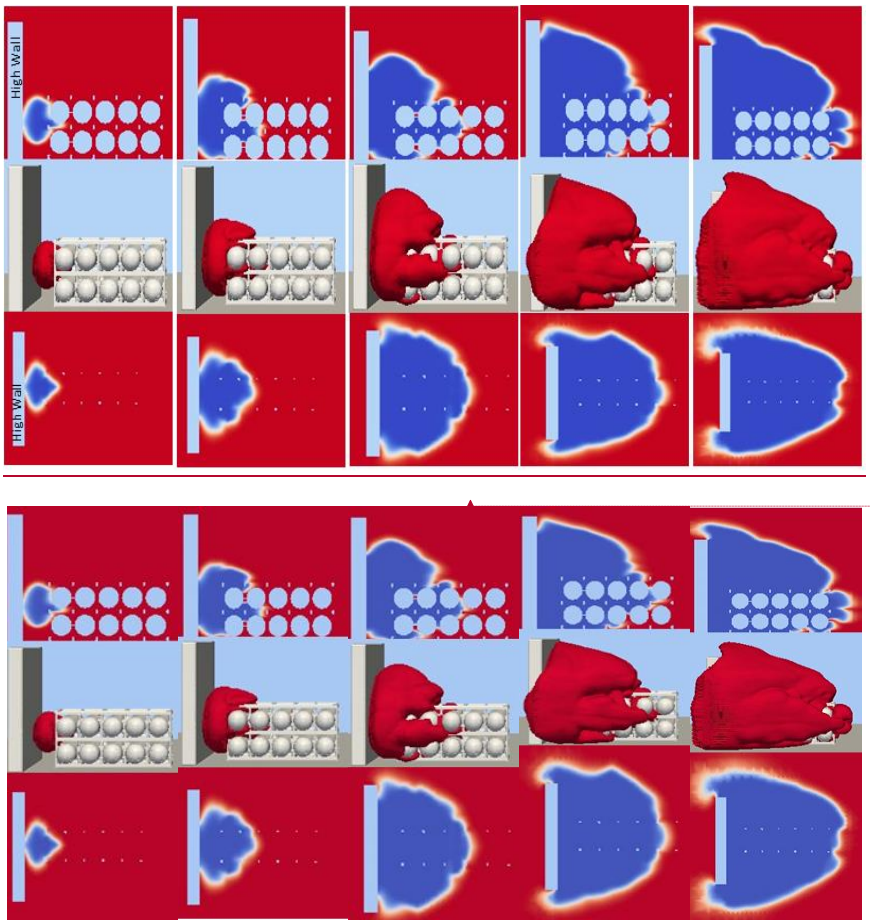

(a) 32 ms (b) 62 ms (c) 92 ms (d) 122 ms (e) 142 ms

Figure ~~7~~5. Profiles of flame propagation at different time instants a) 32 ms, b) 62 ms, c) 92 ms, d) 122 ms and e) 142 ms for CASE-A. Vertical plane at the top and horizontal plane (1.24 m from ground) in the bottom, with corresponding flame (regress variable *b* = 0.5) iso-surface plots in the middle.

Formatted: Centered

Formatted: Font: Not Bold, No underline

Formatted: Centered

As the flame front further propagates, the unburnt gas ahead of the flame is pushed through the cylinders leading to enhancement of turbulence which results in increase in flame speed. This increase in flame speed results in elongation of the leading edge of the flame surface (see top figure 5(a) to (e)). The trailing edge of the flame slowly moves along the length of high wall.

Figure ~~8~~ 6 compares the flame position as a function of time between experiments and simulations. It can be observed that the flame position is slightly underpredicted in simulations ~~at~~ after 3 m from high wall. The flame speed (slope of distance versus time) increases when the flame encounters the congestion and decreases as soon as the flame leaves the congestion. The peak flame speed is underpredicted in simulations (110 m/s) compared with experiments (300 m/s). However, the trends of increase in flame speed as a function of distance is reproduced very well.

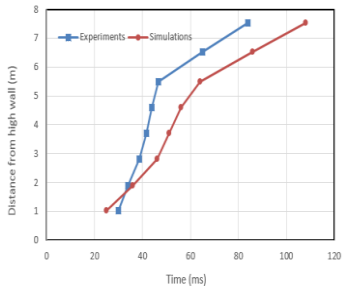

Figure ~~8~~6. Comparison of predicted and measured flame position as a function of time.

The variation of overpressure as a function of time from ignition obtained in experiments and numerical simulations are shown in Figure. ~~9~~7(a)-(~~m~~n). The X-axis in the plots represent the time from the initiation of the spark ignition in 'ms' and Y-axis of the plots represent the overpressure generated in bar. The results are shown here for different probes K1-K4 (Fig. 9(a)-(d)), K5-K7 (Figs. 9(e)-(g)), K8-K11 (Figs. 9(h)-(k)) and KW12-KW14 (Fig. 9(l)-(n)). In general, simulations are able to reproduce the trends observed in experiments.

Formatted: Justified

Formatted: Normal

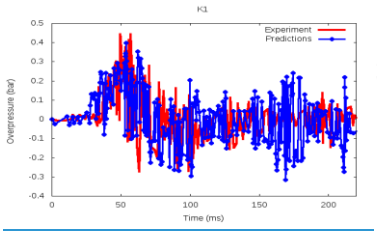
K1
Experiment
Predictions
Overpressure (bar)
Time (ms)

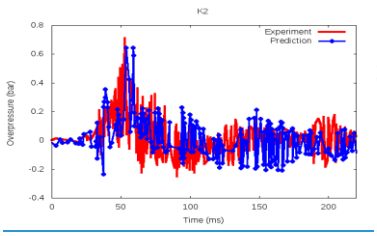
K2
Experiment
Prediction
Overpressure (bar)
Time (ms)

(a)

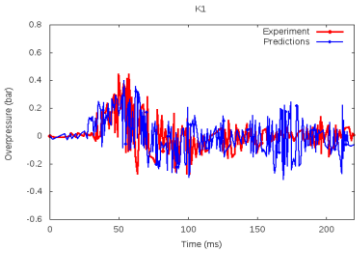
K1
Experiment
Predictions
Overpressure (bar)
Time (ms)

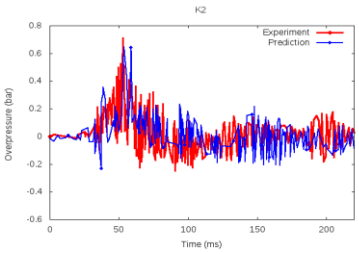
K2
Experiment
Prediction
Overpressure (bar)
Time (ms)

(b)

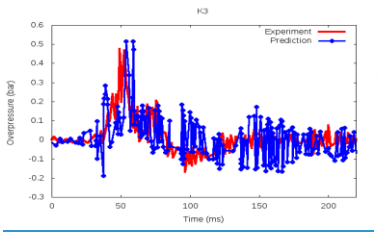
K3
Experiment
Prediction
Overpressure (bar)
Time (ms)

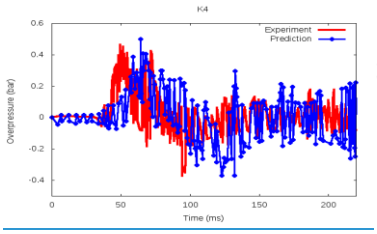
K4
Experiment
Prediction
Overpressure (bar)
Time (ms)

(c)

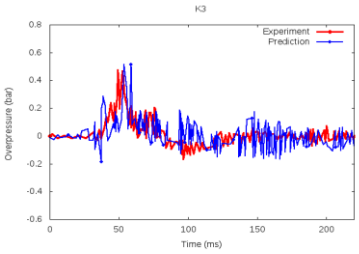
K3
Experiment
Prediction
Overpressure (bar)
Time (ms)

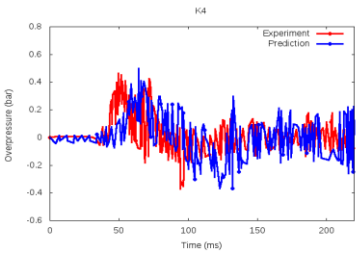
K4
Experiment
Prediction
Overpressure (bar)
Time (ms)

(d)

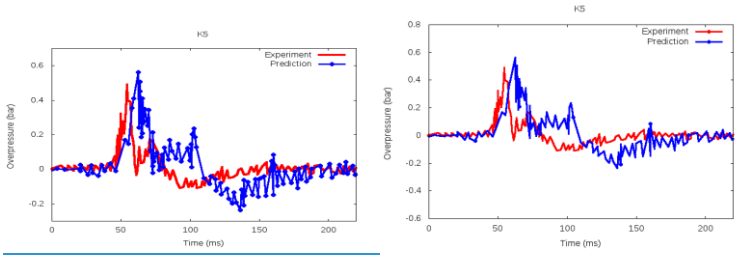
K5
Experiment
Prediction
Overpressure (bar)
Time (ms)

K5
Experiment
Prediction
Overpressure (bar)
Time (ms)

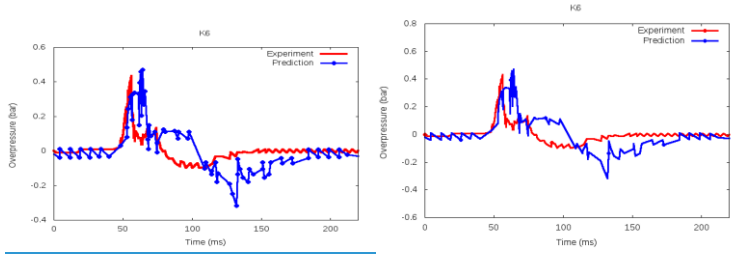
K6
Experiment
Prediction
Overpressure (bar)
Time (ms)

K6
Experiment
Prediction
Overpressure (bar)
Time (ms)

(e) (f)

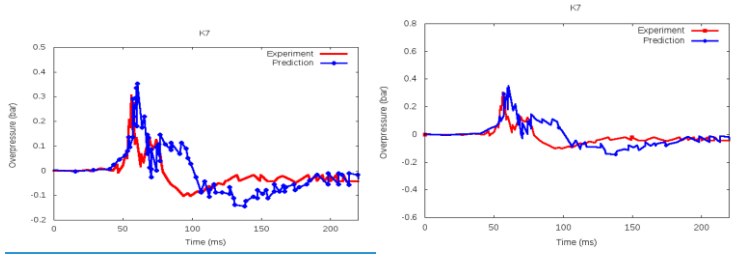
K7
Experiment
Prediction
Overpressure (bar)
Time (ms)

K7
Experiment
Prediction
Overpressure (bar)
Time (ms)

(g)

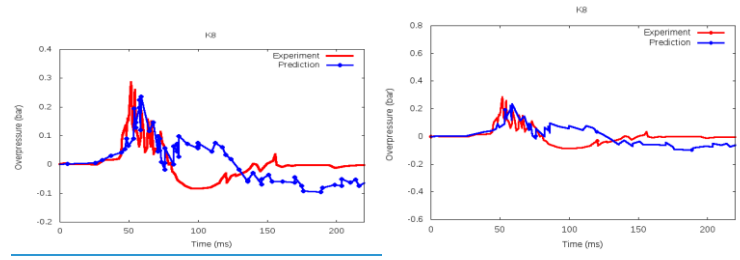
K8
Experiment
Prediction
Overpressure (bar)
Time (ms)

K8
Experiment
Prediction
Overpressure (bar)
Time (ms)

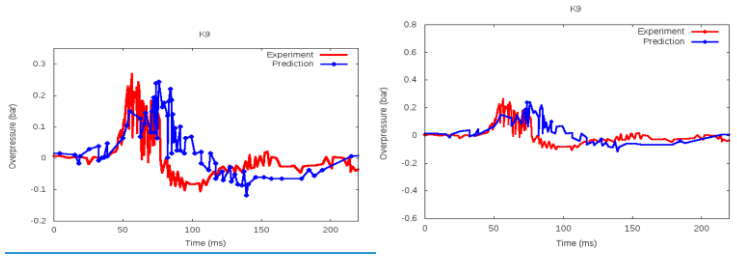
K9
Experiment
Prediction
Overpressure (bar)
Time (ms)

K9
Experiment
Prediction
Overpressure (bar)
Time (ms)

(h)

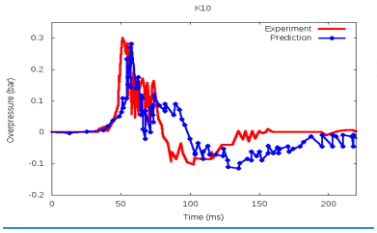
K10
Experiment
Prediction
Overpressure (bar)
Time (ms)

(i)

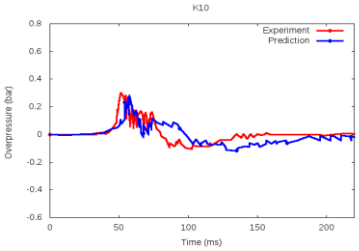
K10
Experiment
Prediction
Overpressure (bar)
Time (ms)

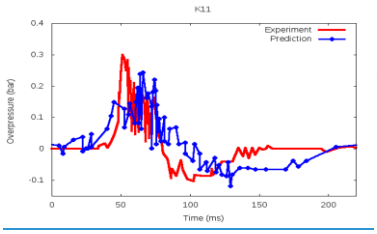
K11
Experiment
Prediction
Overpressure (bar)
Time (ms)

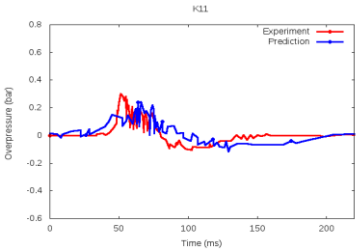
K11
Experiment
Prediction
Overpressure (bar)
Time (ms)

(j)

(k)

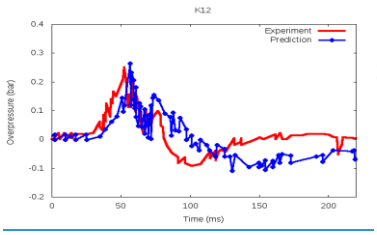
K12
Experiment
Prediction
Overpressure (bar)
Time (ms)

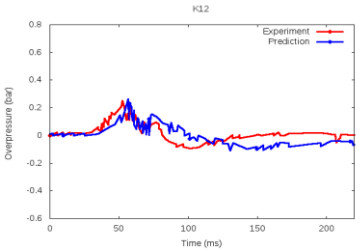
K12
Experiment
Prediction
Overpressure (bar)
Time (ms)

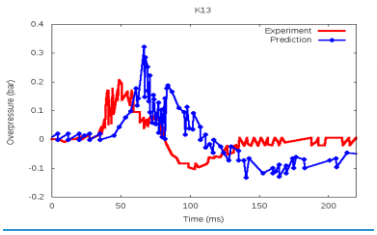
K13
Experiment
Prediction
Overpressure (bar)
Time (ms)

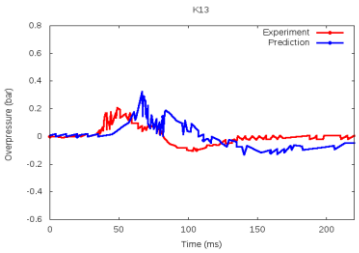
K13
Experiment
Prediction
Overpressure (bar)
Time (ms)

(l)

(m)

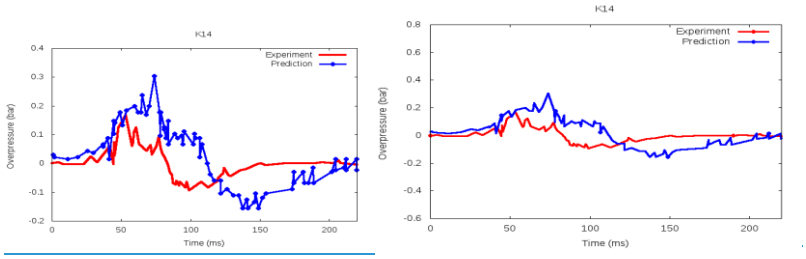

(n)

Figure ~~9~~7. Comparison of predicted and measured overpressure at different probes i.e., a) K1, b) K2, c) K3, d) K4, e) K5, f) K6, g) K7, h) K8, i) K9, j) K10, k) K11, l) KW12, m) KW13 and n) KW14. Probes K1, K2 and K3 are within the congestion, K5, K6, and K7 are in direction away from the High wall. K8, K9, K10 and K11 are in direction parallel to the High wall. KW12, KW13 and KW14 in direction up the High wall.

In order to compare simulations with experiments, the maximum values of overpressures are extracted at each probe. These values are tabulated in Table 3. The simulations are able to predict the experimental maximum value of overpressure within 20 % in the congestion and but the maximum uncertainty of 75–% on the confinement wall. ~~Figure A1~~Figure A1 (in appendix) shows the variation of maximum overpressures as a function of distance (data tabulated in Table 3). The peak overpressure is observed at the K2 probe location, which is within the rig congestion. The observed maximum overpressure within the congestion is higher than observed outside the congestion due to the flame acceleration. ~~Outside the congestion the pressure falls rapidly. Simulations are able predict the location at which overpressure is maximum. Moreover, predictions are able to reproduce the experimental trends of variation of overpressure with distance very well. But on the high wall, numerical predictions show that overpressure increase with distance in contrast to decrease in overpressure with distance in experiments.~~

~~Table 4, shows extracted positive and negative impulses from experiments and simulations. Simulations are able to predict the impulse at probes inside congestion within the uncertainty of 100 %, while at wall it overpredicts the impulse significantly.~~

Formatted: Not Highlight

Table 3. Comparison of overpressure at various probe locations for CASE-A obtained using experiments and simulations.

Formatted: Centered

Sl. No	Monitoring location	Maximum Overpressure (barg)		
		Experiments results	Numerical predictions	% Uncertainty in predictions
Away from High wall				
1	K1	0.44	0.395	-10
2	K2	0.709	0.65	-8
3	K3	0.473	0.514	+9
4	K4	0.464	0.491	+6
5	K5	0.484	0.562	+16
6	K6	0.432	0.462	+7
7	K7	0.306	0.352	+15
Parallel to High wall				

8	K8	0.286	0.233	-19
9	K9	0.267	0.244	-9
10	K10	0.297	0.282	-5.0
11	K11	0.209	0.242	+16
On the High wall				
12	KW12	0.25	0.262	+5
13	KW13	0.206	0.321	+56
14	KW14	0.172	0.302	+76

Outside the congestion the pressure falls rapidly. Simulations are able to predict the location at which overpressure is maximum. Moreover, predictions are able to reproduce the experimental trends of variation of overpressure with distance very well. But on the high wall, numerical predictions show that overpressure increase with distance in contrast to decrease in overpressure with distance in experiments. Table 4, shows extracted positive and negative impulses from experiments and simulations. Simulations are able to predict the impulse at probes inside congestion within the uncertainty of 100 %, while at wall it overpredicts the impulse significantly.

Formatted: Centered

Table 4. Comparison of positive and negative impulse at various probe locations for CASE-A obtained using experiments and simulations.

Formatted Table

		Experiments		Predictions		% Uncertainty in predictions	
Sl.no	Probe location	Positive impulse (bar.ms)	Negative impulse (bar.ms)	Positive impulse (bar.ms)	Negative impulse (bar.ms)	Positive impulse	Negative impulse
Away from the High wall							
1	K1	9.04	-6.99	9.77	-9.79	+8	+40
2	K2	11.73	-6.93	14.62	-14.28	+25	+106
3	K3	7.23	-4.36	11.7	-11.42	+62	+162
4	K4	11.16	-7.71	17.62	-15.11	+58	+96
5	K5	6.26	-4.03	11.29	-9.02	+80	+124
6	K6	4.27	-3.98	8.57	-12.43	+101	+212
7	K7	3.01	-8.78	6.25	-12.29	+108	+40
Parallel to High wall							
8	K8	3.91	-3.92	6.94	-13.65	+77	+248
9	K9	4.32	-5.55	8.29	-6.15	+92	+11
10	K10	5.09	-4.08	5	-9.83	-2	+141
11	K11	5.09	-4.08	8.29	-6.15	+63	+51
On the High wall							

12	KW12	6.39	-3.14	6.17	-13.68	-3	+336
13	KW13	4.97	-4.62	7.54	-16.73	+52	+262
14	KW14	3.52	-3.64	12.49	-8.97	+255	+146

5.2 CASE–B: Two wall scenario (Low wall ignition)-CFD model validation

Flame and pressure dynamics obtained using simulations are compared against experiments for CASE-B in this section.

Figure ~~10~~8, shows the contours and iso-surfaces of regress variable, *b* at different time instants. Again, ~~T~~top part of figure shows the contours on a vertical plane and bottom figure shows the contours on a horizontal plane. Figure in the middle shows iso-surface of regress variable corresponding to *b*=0.5.

The ignition in this simulation is close to the Low wall, which makes the flame enter the rig congestion at the middle, leading to the flame acceleration along the length of the cylinders and radially outwards. Flame wrinkling produced by these cylinders is ~~less~~ more in the present case compared to previous case (compare Fig. ~~10~~ 8(~~d~~c) with Fig ~~7~~ 5(~~e~~c-d)), because of ~~less~~ more turbulence generation, when unburnt gases travels along the length of the cylinders.

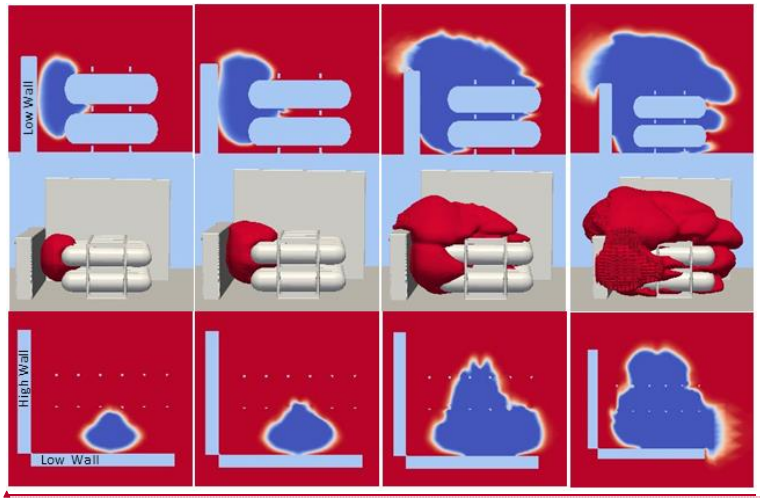

Formatted: List Paragraph

Formatted: Font: Not Bold, No underline

Formatted: Centered

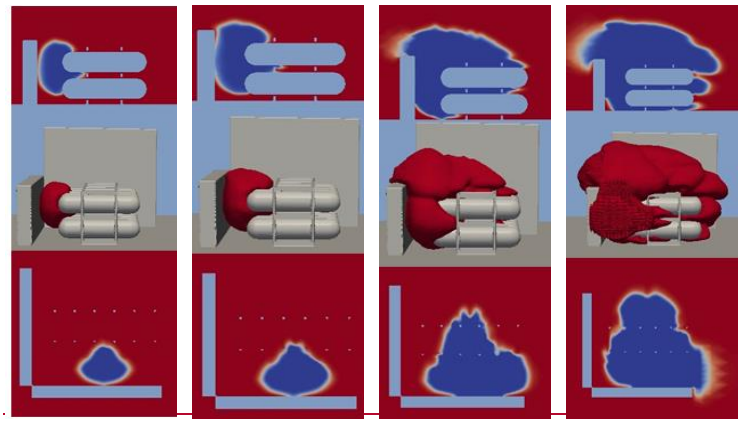

(a) 31 ms (b) 43 ms (c) 55 ms (d) 68 ms

Formatted: Centered

Figure ~~10~~8. Profiles of flame propagation at different time instants i.e. a) 31 ms, b) 43 ms, c) 55 ms and d) 68 ms for CASE-B. Vertical plane at the top and horizontal plane in the bottom, with corresponding flame (b = 0.5) iso-surface plots in the middle.

Figure ~~11~~ 9 compares the flame position as a function of time between experiments and simulations. It can be observed that flame position and flame speed is slightly underpredicted in simulations. However, the trends of increase in flame position with distance are correctly predicted by simulations.

Formatted: Font: Not Bold, Not Italic, No underline

Formatted: Centered

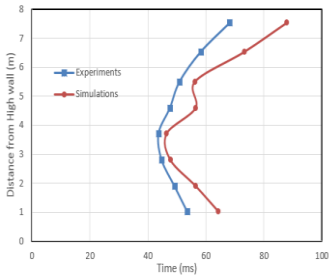

Figure ~~11~~9. Comparison of predicted and measured flame position as a function of time.

The variation of overpressure as a function of time from ignition obtained in experiments and numerical simulations are shown in Figs. 1~~2~~0(a)-(m). The X-axis in the plots represent the time from the initiation of the spark ignition in 'ms' and Y-axis of the plots represent the overpressure generated in bar. The results are shown here for different probes K1-K4 (Figs. ~~12~~10(a)-(d)), K5-K7 (Figs. ~~12~~10(e)-(g)), K8-K11 (Figs. ~~12~~10(h)-(j)) and KW12-KW14 (Figs. ~~12~~10(k)-(m)). The figure 10(m) experimental data is not available due to sensor failure in the experiment. In general, simulations are able to reproduce the trends observed in experiments.

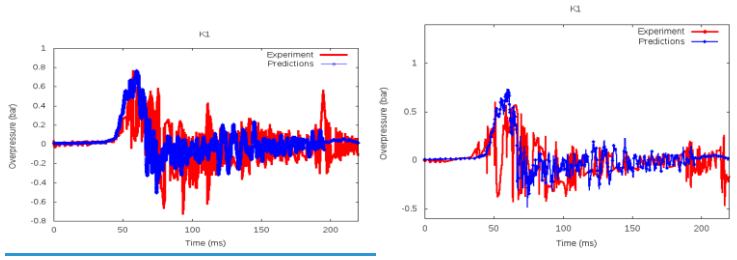
K1
Experiment
Predictions
Overpressure (bar)
Time (ms)

K1
Experiment
Predictions
Overpressure (bar)
Time (ms)

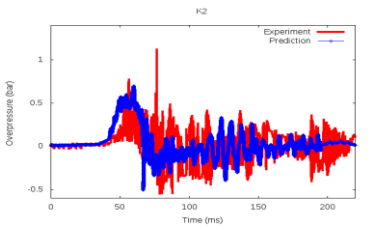
K2
Experiment
Prediction
Overpressure (bar)
Time (ms)

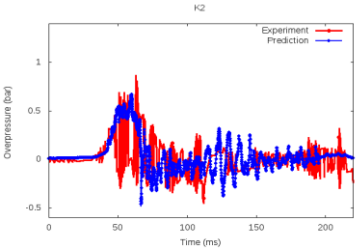
K2
Experiment
Prediction
Overpressure (bar)
Time (ms)

(a)

(b)

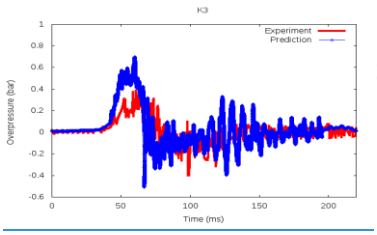
K3
Experiment
Prediction
Overpressure (bar)
Time (ms)

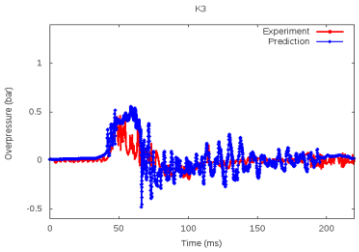
K3
Experiment
Prediction
Overpressure (bar)
Time (ms)

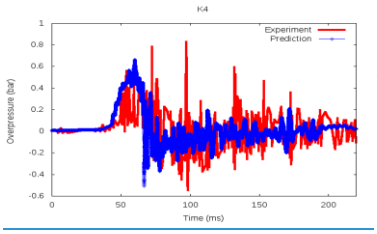
K4
Experiment
Prediction
Overpressure (bar)
Time (ms)

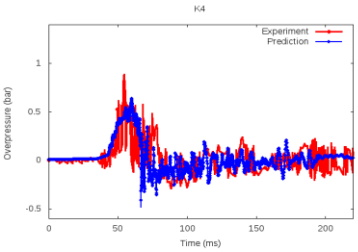
K4
Experiment
Prediction
Overpressure (bar)
Time (ms)

(c)

(d)

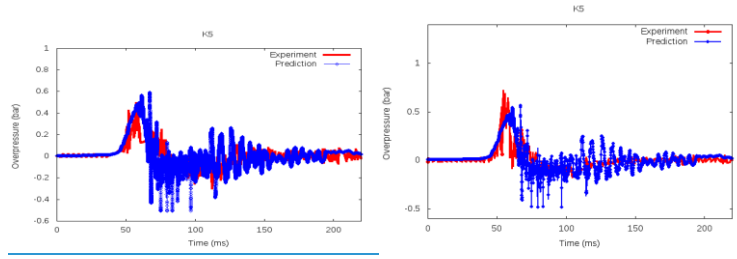
K5
Experiment
Prediction
Overpressure (bar)
Time (ms)

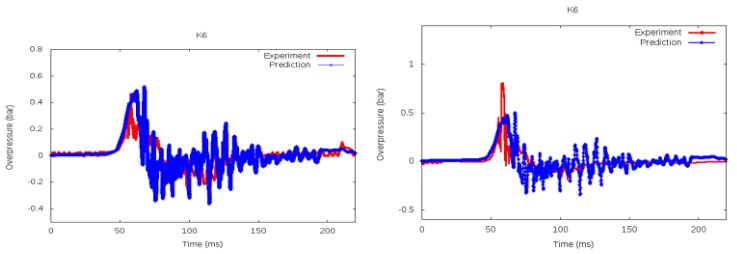
K6
Experiment
Prediction
Overpressure (bar)
Time (ms)

(e) (f)

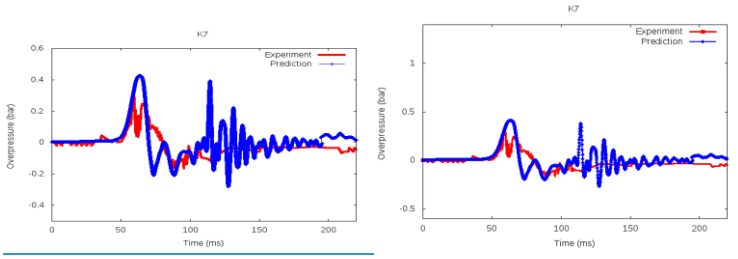
K7
Experiment
Prediction
Overpressure (bar)
Time (ms)

(g)

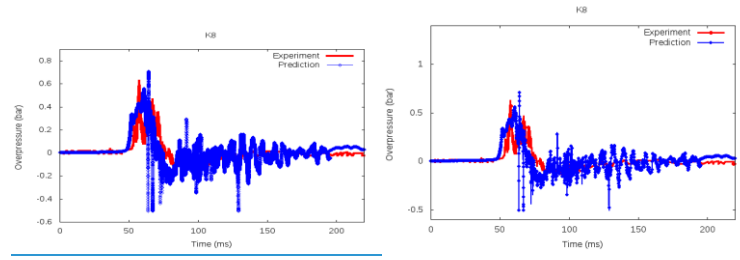
K8
Experiment
Prediction
Overpressure (bar)
Time (ms)

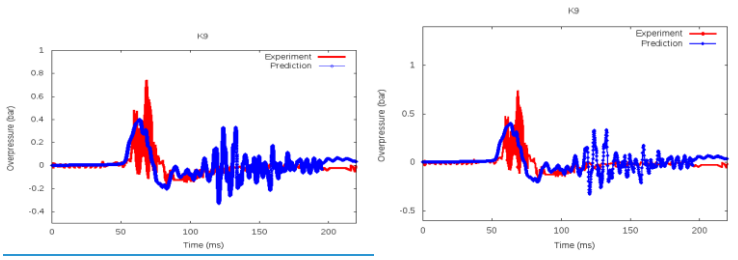
K9
Experiment
Prediction
Overpressure (bar)
Time (ms)

(h) (i)

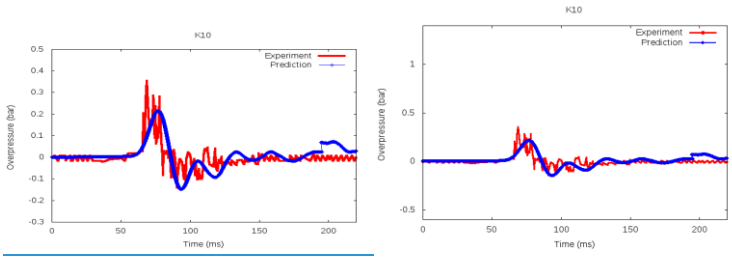

(j)

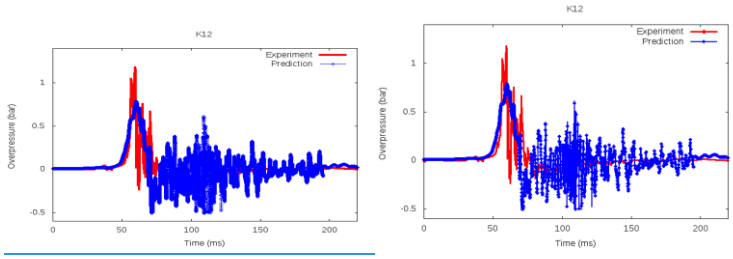

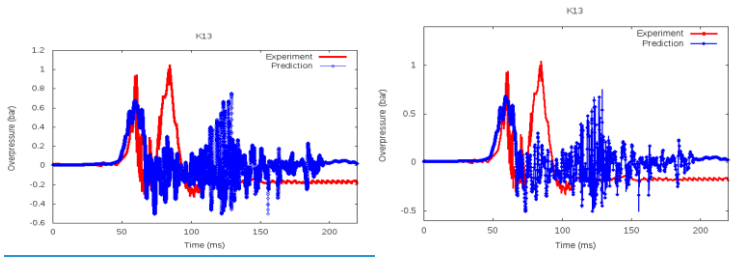

(k) (l)

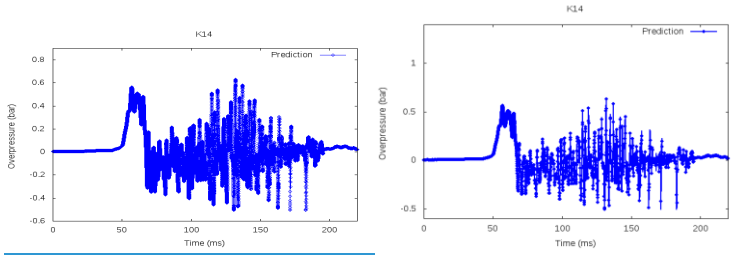

(m)

Figure ~~12~~10. Comparison of predicted and measured overpressure at different probes i.e., a) K1, b) K2, c) K3, d) K4, e) K5, f) K6, g) K7, h) K8, i) K9, j) K10, k) KW12, l) KW13 and m) KW14. Probes K1, K2 and K3 are within the congestion, K5, K6, and K7 are in direction away from the High wall, K8, K9 and K10 are in direction parallel to the High wall, KW12, KW13 and KW14 in direction up the High wall.

In order to compare simulations with experiments, maximum values of overpressures are extracted at each probe. These values are tabulated in Table 5. The simulations are able to predict the experimental maximum value of overpressure at each probe, within the maximum uncertainty of 47 %. Figure A2 (in appendix) shows the variation of maximum overpressures as a function of distance. The peak overpressure is observed at the KW12, which is on the High wall. Within the congestion, the peak overpressure is at the K1 location. Outward flame acceleration and the High wall confining the pressure wave leads to the peak overpressure at K2 probe location. There is also significant flame acceleration in the parallel to High wall direction, therefore K8 also recorded higher overpressures . Simulations are able to reproduce the location at which peak overpressure is observed and trends of variation of overpressure as a function of distance. Table 6, shows extracted positive and negative impulses from experiments and simulations. Simulations are able to reproduce the experimental impulse within the uncertainty of 130 % (inside congestion) and 145 % (on the wall), respectively.

Table 5. Comparison of overpressure at various probe locations for CASE-B obtained using experiments and simulations. * not measured in experiments.

Sl. No	Monitoring location	Maximum Overpressure (barg)		
		Experiments results	Numerical predictions	% Uncertainty in predictions
Away from High wall				
1	K1	0.76	0.737	-3
2	K2	0.763	0.674	-12
3	K3	0.389	0.56	+44
4	K4	0.775	0.645	-17
5	K5	0.492	0.557	+13
6	K6	0.464	0.505	+9
7	K7	0.348	0.411	+18
Parallel to High wall				
8	K8	0.63	0.682	+8
9	K9	0.735	0.39	-47
10	K10	0.358	0.21	-41
On the High wall				
12	KW12	1.174	0.764	-35
13	KW13	1.03	0.711	-31
14	KW14	*	0.613	*

Table 6. Comparison of positive and negative impulse at various probe locations for CASE-B obtained using experiments and simulations. * not measured in experiments.

		Experiment		Predictions		% Uncertainity in predictions	
Sl. No	Probe location	Positive impulse (bar.ms)	Negative impulse (bar.ms)	Positive impulse (bar.ms)	Negative impulse (bar.ms)	Positive impulse	Negative impulse
Away from High wall							
1	K1	16.75	-17.14	14.56	-8.31	-13	-52
2	K2	18.66	-15.38	16.08	-9.1	-14	-41
3	K3	9.32	-7.44	16.08	-9.1	+73	+22

Formatted Table

4	K4	17.13	-12.37	13.34	-7.87	-22	-36
5	K5	7.65	-6.2	10.81	-8.24	+41	+33
6	K6	7.53	-5.5	9.32	-7.03	+24	+28
7	K7	3.72	-10.43	8.64	-6.58	+132	-37
Parallel to High wall							
8	K8	6.52	-4.9	9.76	-7.26	+50	+48
9	K9	3.99	-6.62	9.27	-7.41	+132	+12
10	K10	3	-3.2	5.55	-3.25	+85	+2
On the High wall							
12	KW12	9.1	-4.33	15.61	-10.58	+72	+144
13	KW13	14.58	-34.53	14.02	-10.11	-4	-71
14	KW14	*	*	12.79	-10.38	*	*

Formatted: Font: Bold

Formatted: Font: Bold

~~In order to compare simulations with experiments, maximum values of overpressures are extracted at each probe. These values are tabulated in Table 5. The simulations are able to predict the experimental maximum value of overpressure at each probe, within the maximum uncertainty of 47 %. Figure A2 shows the variation of maximum overpressures as a function of distance. The peak overpressure is observed at the KW12, which is on the High wall. Within the congestion, the peak overpressure is at the K1 location. Outward flame acceleration and the High wall confining the pressure wave leads to the peak overpressure at K2 probe location. There is also significant flame acceleration in the parallel to High wall direction, therefore K8 also recorded higher overpressures. Simulations are able to reproduce the location at which peak overpressure is observed and trends of variation of overpressure as a function of distance. Table 6 shows extracted positive and negative impulses from experiments and simulations. Simulations are able to reproduce the experimental impulse within the uncertainty of 130 % (inside congestion) and 145 % (on the wall), respectively.~~

5.3 CASE–C: Two wall scenario (High wall ignition)-CFD model validation

Formatted: Font: Not Italic

Flame and pressure dynamics obtained using simulations are compared against experiments for CASE-C in this section.

Figure ~~13~~ 11 shows the contours and iso-surfaces of regress variable, *b* at different time instants. Again, ~~T~~top figure shows the contours on a vertical plane and bottom figure shows the contours on a horizontal plane. Figure in the middle shows iso-surface of regress variable corresponding to *b*=0.5. Flame behaviour is similar as in CASE-A until the flame reaches the low wall. When it reaches the low wall, free expansion of the flame is prevented leading to non-symmetric flame shape (compare flame shapes in bottom Fig. ~~13~~11(d) and Fig. ~~7~~5(e)).

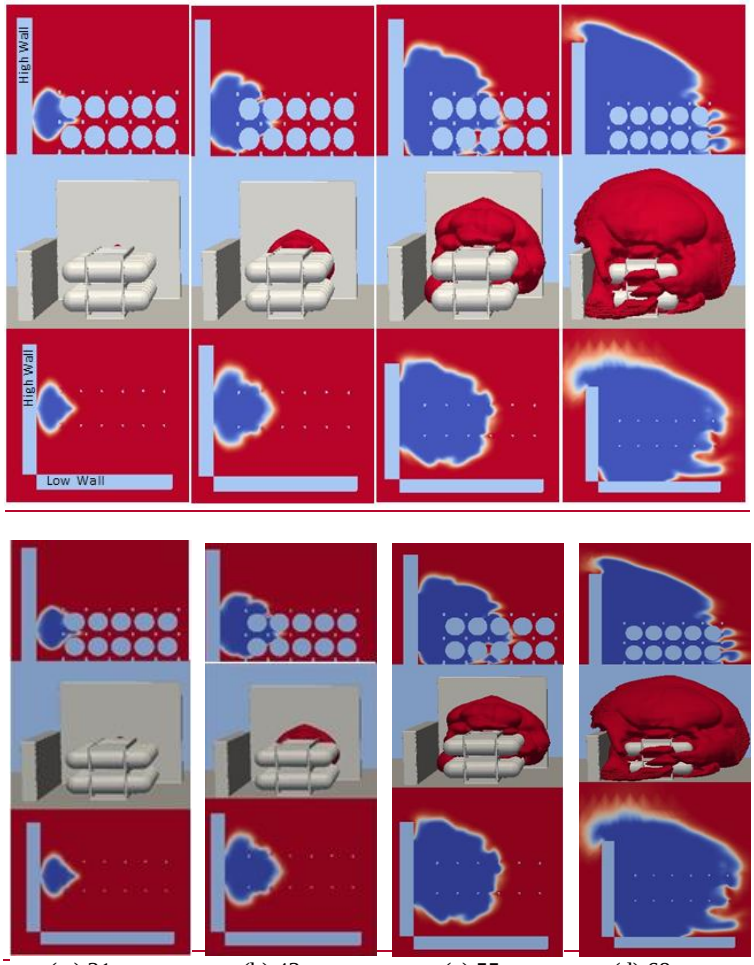

(a) 31 ms (b) 43 ms (c) 55 ms (d) 68 ms

Figure ~~13~~11. Profiles of flame propagation at different time instants i.e. a) 31 ms, b) 43 ms, c) 55 ms and d) 68 ms for CASE-C. Vertical plane at the top and horizontal plane in the bottom, with corresponding flame (b = 0.5) iso-surface plots in the middle.

~~Figure 14 compares the flame position as a function of time between experiments and simulations. It can be observed that the flame position and flame speed is slightly underpredicted in simulations.~~

Formatted: Centered

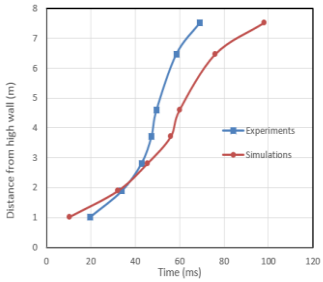

Figure ~~14~~12. Comparison of predicted and measured flame position as a function of time.

Formatted: Centered

Formatted: Centered

Formatted: List Paragraph, Justified

Formatted: List Paragraph

Figure 12 compares the flame position as a function of time between experiments and simulations. It can be observed that the flame position and speed in later part of the flame propagation seems to be underpredicted in simulations.

The variation of overpressure as a function of time from ignition obtained in experiments and numerical simulations are shown in Figs. ~~15~~13(a)-(m). The X-axis in the plots represent the time from the initiation of the spark ignition in 'ms' and Y-axis of the plots represent the overpressure generated in bar. The results are shown here for different probes K1-K4 (Figs. (a)-(d)), K5-K7 (Figs.13-(e)-(g)), K8-K11 (Figs.13-(h)-(j)) and KW12-KW14 (Figs.-13(k)-(m)). In general, simulations are able to reproduce the trends observed in experiments.

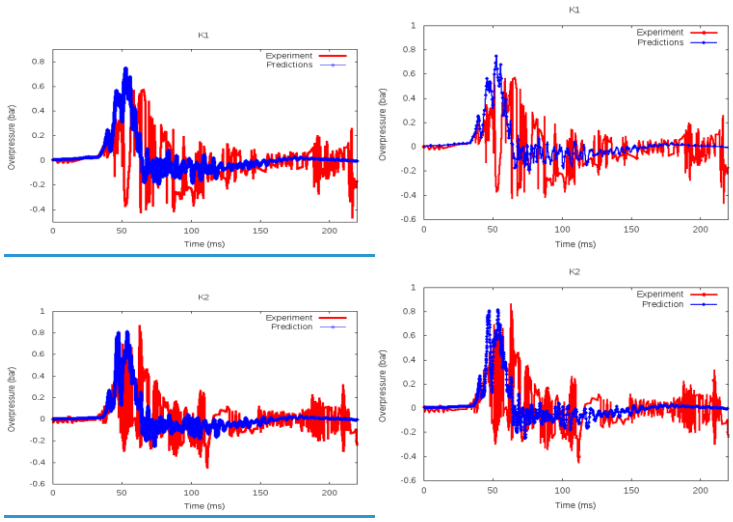

(a) (b)

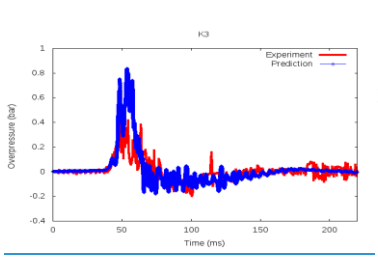
K3
Experiment
Prediction
Overpressure (bar)
Time (ms)

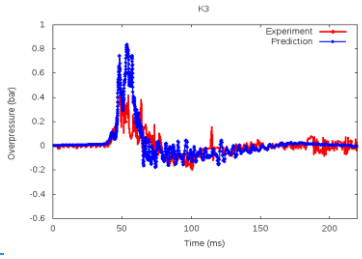
K3
Experiment
Prediction
Overpressure (bar)
Time (ms)

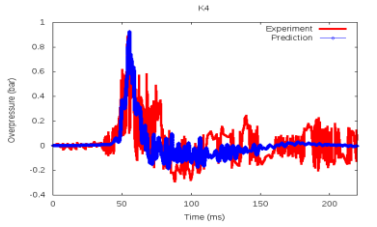
K4
Experiment
Prediction
Overpressure (bar)
Time (ms)

(c)

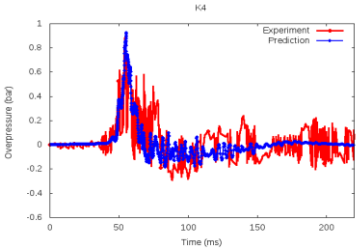
K4
Experiment
Prediction
Overpressure (bar)
Time (ms)

(d)

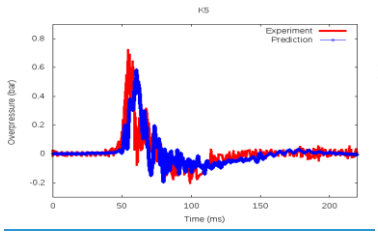
K5
Experiment
Prediction
Overpressure (bar)
Time (ms)

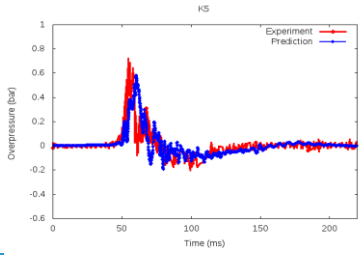
K5
Experiment
Prediction
Overpressure (bar)
Time (ms)

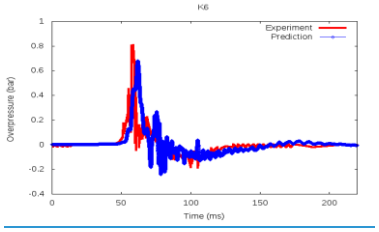
K6
Experiment
Prediction
Overpressure (bar)
Time (ms)

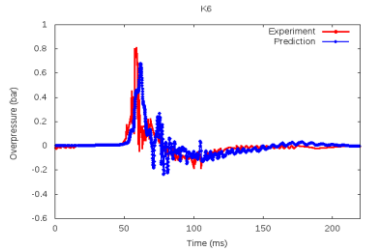
K6
Experiment
Prediction
Overpressure (bar)
Time (ms)

(e)

(f)

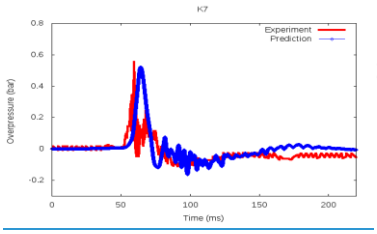
K7
Experiment
Prediction
Overpressure (bar)
Time (ms)

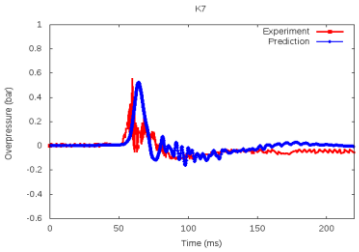
K7
Experiment
Prediction
Overpressure (bar)
Time (ms)

(g)

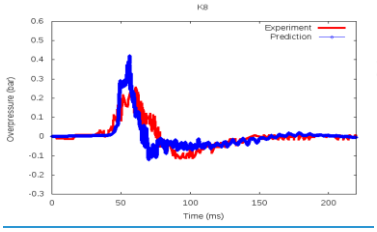
K8
Experiment
Prediction
Overpressure (bar)
Time (ms)

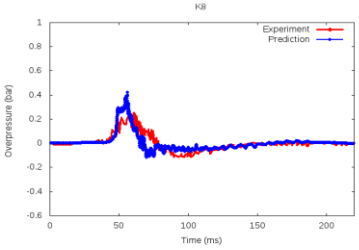
K8
Experiment
Prediction
Overpressure (bar)
Time (ms)

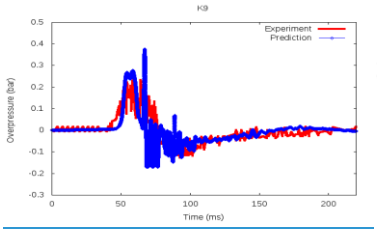
K9
Experiment
Prediction
Overpressure (bar)
Time (ms)

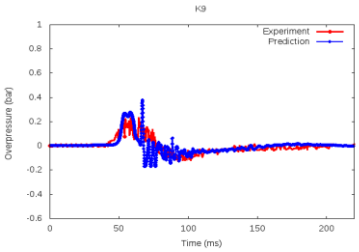
K9
Experiment
Prediction
Overpressure (bar)
Time (ms)

(h) (i)

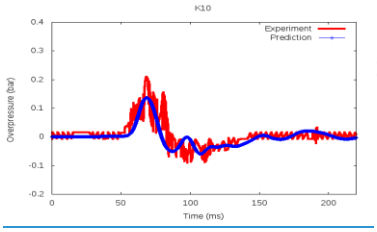
K10
Experiment
Prediction
Overpressure (bar)
Time (ms)

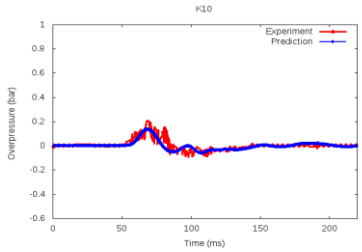
K10
Experiment
Prediction
Overpressure (bar)
Time (ms)

(j)

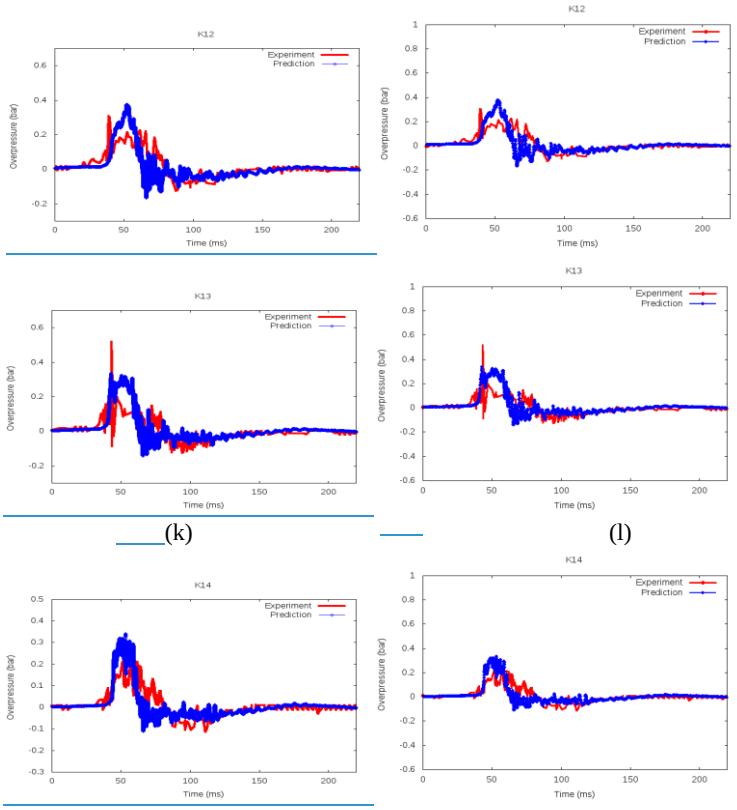

(k) (l)

(m)

Figure 1513. Comparison of predicted and measured overpressure at different probes i.e., a) K1, b) K2, c) K3, d) K4, e) K5, f) K6, g) K7, h) K8, i) K9, j) K10, k) KW12, l) KW13 and m) KW14. Probes K1, K2 and K3 are within the congestion, K5, K6, and K7 are in direction away from the High wall, K8, K9 and K10 are in direction parallel to the High wall, KW12, KW13 and KW14 in direction up the High wall.

In order to compare simulations with experiments, maximum values of overpressures are extracted at each probe. These values are tabulated in Table 7. The simulations are able to predict the experimental maximum value of overpressure at each probe, within the uncertainty of 56 %. Figure A3 (in appendix) shows the plots of maximum overpressures as a function of distance. The peak overpressure is observed at the K4, which is within the congestion.

Table 7. Comparison of overpressure at various probe locations for CASE-C obtained using experiments and simulations.

Formatted: Centered

Sl. No	Monitoring location	Maximum Overpressure (barg)		
		Experiments results	Numerical predictions	% Uncertainity in predictions
Away from High wall				

1	K1	0.596	0.754	+27
2	K2	0.866	0.674	-22
3	K3	0.457	0.835	+83
4	K4	0.882	0.919	+4
5	K5	0.717	0.695	-3
6	K6	0.801	0.527	-34
7	K7	0.557	0.411	-26
Parallel to High wall				
8	K8	0.25	0.42	+68
9	K9	0.268	0.379	+41
10	K10	0.209	0.13	-38
On the High wall				
12	KW12	0.307	0.378	+23
13	KW13	0.516	0.333	-35
14	KW14	0.216	0.337	+56

Table 8. Comparison of impulse at various probe locations for CASE-C obtained using experiments and simulations.

		Experiment		Predictions		% Uncertainity in predictions	
Sl.no	Probe location	Positive impulse (bar.ms)	Negative impulse (bar.ms)	Positive impulse (bar.ms)	Negative impulse (bar.ms)	Positive impulse	Negative impulse
Away from High wall							
1	K1	13.55	-17.48	11.11	-5.83	-18	-67
2	K2	14.7	-13.14	10.79	-5.89	-27	-55
3	K3	7.03	-6.37	9.53	-5.69	+36	-11
4	K4	17.11	-11.79	8.35	-5.56	-51	-53
5	K5	7.09	-5.49	6.39	-5.14	-10	-6
6	K6	5.06	-4.69	6.29	-5.22	+24	+11
7	K7	3.54	-10.04	5.29	-5.01	+49	-50
Parallel to High wall							
8	K8	4.85	-4.43	4.4	-3.77	-9	-15
9	K9	3.98	-4.72	3.81	-4.37	-4	-7
10	K10	3.93	-2.11	2.39	-2.41	-39	+14
On the High wall							
12	KW12	7.45	-3.39	6.61	-3.6	-11	+6
13	KW13	4.73	-4.28	6.21	-3.35	+31	-22
14	KW14	4.93	-3.48	4.99	-2.92	+1	-16

~~In order to compare simulations with experiments, maximum values of overpressures are extracted at each probe. These values are tabulated in Table 7. The simulations are able to predict the experimental maximum value of overpressure at each probe, within the uncertainty~~

~~of 56 %. Figure A3 shows the plots of maximum overpressures as a function of distance. The peak overpressure is observed at the K4, which is within the congestion.~~ The location of peak overpressure is reproduced by simulations very well. Moreover, simulations are able to predicts the variation of maximum overpressure with distance well.
Table 8, shows the comparison of positive and negative impulses obtained using experiments and simulations. Simulations are able to reproduce impulses within the accuracy of 67 %.

5.4 CASE–D: Three wall scenario (Low wall ignition)- CFD model numerical investigation

Flame and pressure dynamics obtained using simulations are presented for CASE-D in this section. The geometry for this case is same as CASE B with addition of third wall.

Figure ~~16~~ 14 shows the contours and iso-surfaces of regress variable, *b* at different time instants. Top figure shows the contours on a vertical plane and bottom figure shows the contours on a horizontal plane. Figure in the middle shows iso-surface of regress variable corresponding to *b*=0.5. Since ignition in this case is close to low wall, the flame behavior is similar to CASE-B until flame reaches the third wall. Free expansion of the flame is prevented by walls leading to flame moving outwards (~~see~~ top and bottom picture in Fig. ~~16~~ 8(d)).

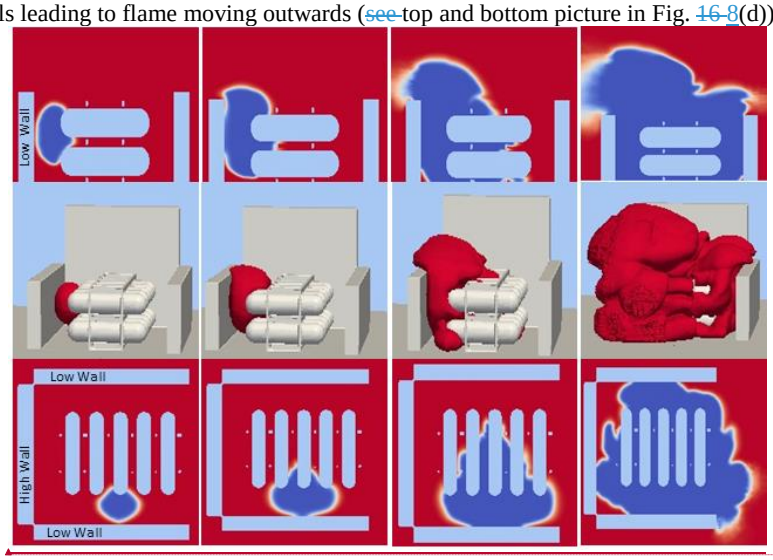

Formatted: Font: Not Bold, No underline

Formatted: Centered

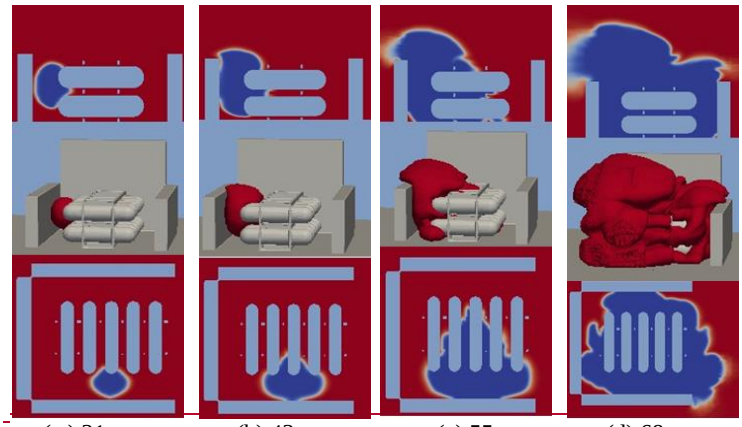

(a) 31 ms (b) 43 ms (c) 55 ms (d) 68 ms

Figure ~~16~~14. Profiles of flame propagation at different time instants i.e. a) 31 ms, b) 43 ms, c) 55 ms and d) 68 ms for CASE-D. Vertical plane at the top and horizontal plane in the bottom, with corresponding flame (b = 0.5) iso-surface plots in the middle.

The variation of overpressure as a function of time from ignition obtained in experiments and numerical simulations are shown in Figs. 15(a)-(j). The X-axis in the plots represent the time from the initiation of the spark ignition in 'ms' and Y-axis of the plots represent the overpressure generated in bar. The results are shown here for different probes K1-K4 (Figs. (a)-(d)), K5-K7 (Figs.15(e)-(g)) and KW12-KW14 (Figs.15(h)-(j)). In general, simulations are able to reproduce the trends observed in experiments.

Formatted: Justified, Indent: Left: 0 cm, First line: 0 cm

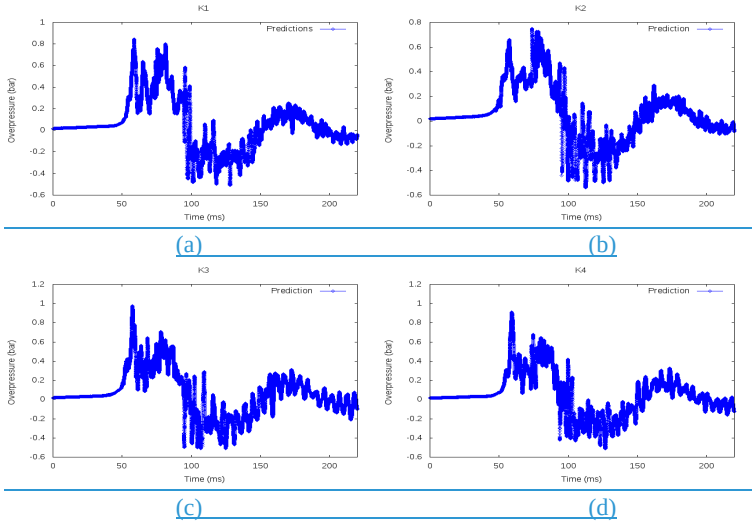

(a) (b)

(c) (d)

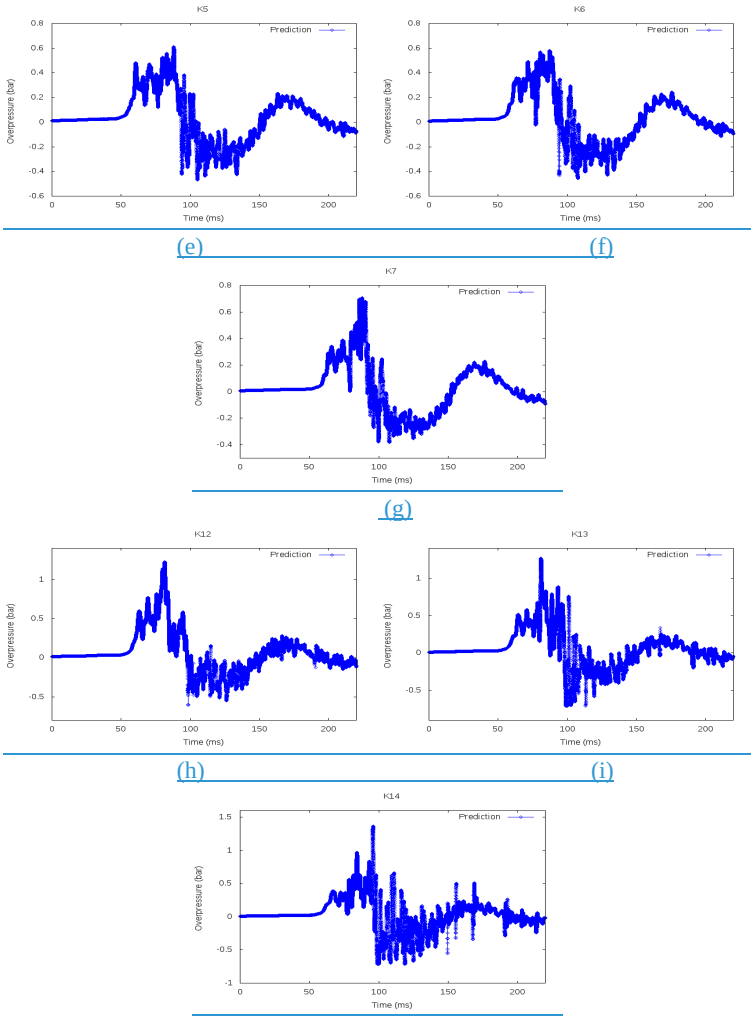

Figure 15. The predicted overpressure at different probes i.e., a) K1, b) K2, c) K3, d) K4, e) K5, f) K6, g) K7, h) KW12, i) KW13 and j) KW14. Probes K1, K2 and K3 are within the congestion, K5, K6, and K7 are in direction away from the High wall, KW12, KW13 and KW14 in direction up the High wall.

Figure ~~17~~ 16 shows the flame position as a function of time obtained using simulations. Flame position is compared for two walls (CASE-B) and three walls (CASE-D) scenario. It can be observed that the trends of flame positions are very similar.

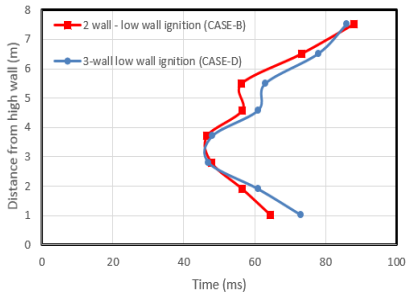

Figure ~~17~~16. Comparison of predicted flame position as a function of time obtained using simulation for CASE-B and D.

Table 9. Maximum overpressure at various probe locations for CASE-D obtained using ~~experiments~~numerical simulations.

Sl. No.	Monitoring Location	Maximum overpressure Numerical predictions (barg)
Away from High wall		
1	K1	0.842
2	K2	0.745
3	K3	0.985
4	K4	0.904
5	K5	0.611
6	K6	0.585
7	K7	0.710
On the High wall		
8	KW12	1.229
9	KW13	1.28
10	KW14	1.388

Maximum values of overpressures are extracted at each probe. These values are tabulated in Table 9. Figure A4 (in appendix) shows the plots of maximum overpressure as a function of distance at different probes. The peak overpressure is observed at the KW14, which is on the High wall while, within the congestion the peak overpressure is at the K3 probe location. It is worth noting that the observed peak overpressure is higher for 3 wall case than for 2 wall case. This essentially means that overpressure increases with confinement, this is further discussed later.

5.5 CASE–E: Three wall scenario (High wall ignition)-CFD model numerical investigation

Flame and pressure dynamics obtained using simulations are presented for CASE-E in this section. The geometry for this case is same as CASE-C with addition of third wall.

Formatted: Font: Italic

Formatted: Font: Not Bold, Italic

Figure ~~18~~ 17 shows the contours and iso-surfaces of regress variable, *b* at different time instants. Top figure shows the contours on a vertical plane and bottom figure shows the contours on a horizontal plane. Figure in the middle shows iso-surface of regress variable corresponding to *b*=0.5. Since ignition in this case to close to High wall, flame behavior is similar to CASE-A and CASE-C until flame reaches the third wall. .

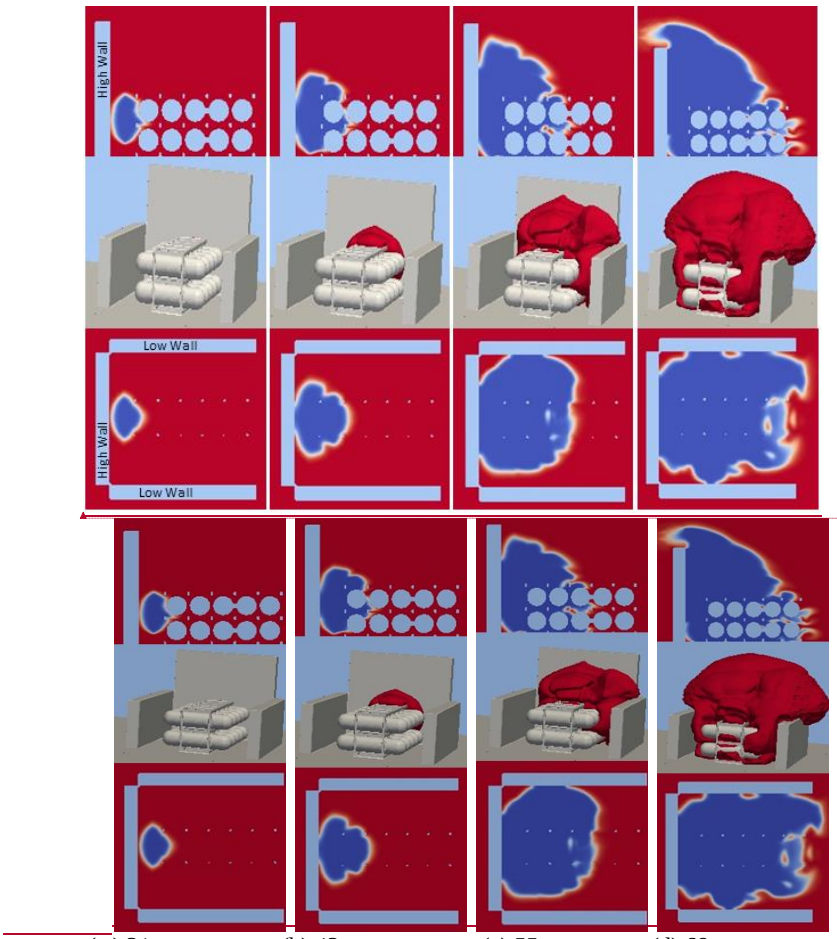

(a) 31 ms (b) 43 ms (c) 55 ms (d) 68 ms

Figure ~~18~~17. Profiles of flame propagation at different time instants i.e. a) 31 ms, b) 43 ms, c) 55 ms and d) 68 ms for CASE-E. Vertical plane at the top and horizontal plane in the bottom, with corresponding flame (*b* = 0.5) iso-surface plots in the middle.

Figure ~~19~~ 18 shows the flame position as a function of time obtained using simulations. Flame position is compared for one wall (CASE-A), two walls (CASE-B) and three walls (CASE-E) case. It can be observed that the trends of flame positions are similar.

Formatted: Font: Not Bold, No underline

Formatted: Centered

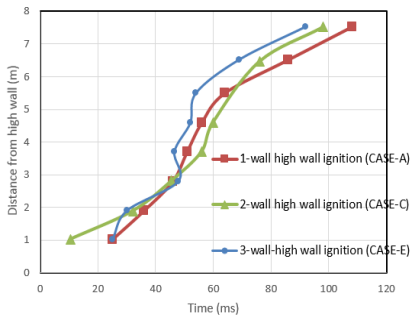

Figure ~~19~~18. Comparison of predicted flame position as a function of time for CASE-A, C and E for high wall ignition.~~.~~

The overpressure as a function of time from ignition obtained in experiments and numerical simulations at various probe locations are shown in Figs. 19(a)-(j). The X-axis in the plots represent the time from the initiation of the spark ignition in 'ms' and Y-axis of the plots represent the overpressure generated in bar. The results are shown here for different probes K1-K4 (Figs.19(a)-(d)), K5-K7 (Figs.19(e)-(g)) and KW12-KW14 (Figs.19(h)-(j)). In general, simulations are able to reproduce the trends observed in experiments.

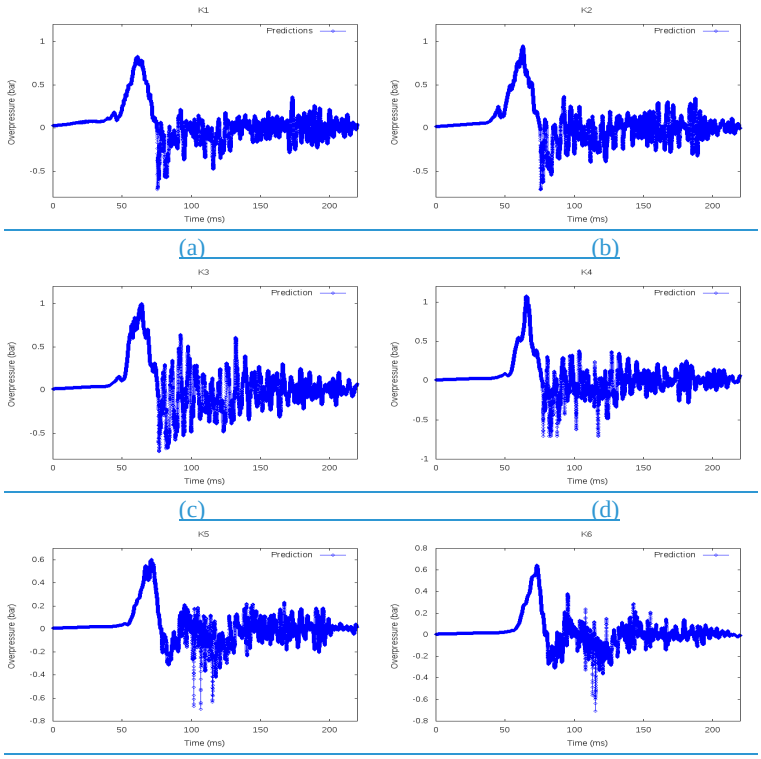

(a) (b)

(c) (d)

Formatted: Centered

Formatted: Justified

(e) (f)

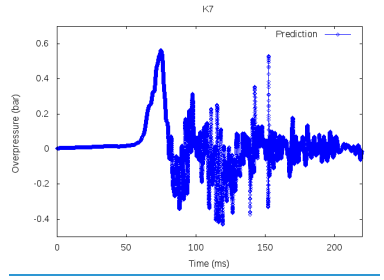

(g)

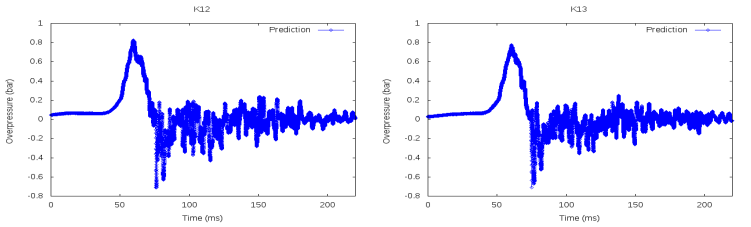

(h) (i)

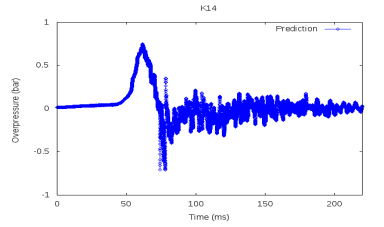

(j)

Figure 19. The predicted overpressure at different probes i.e., a) K1, b) K2, c) K3, d) K4, e) K5, f) K6, g) K7, h) KW12, i) KW13 and j) KW14. Probes K1, K2 and K3 are within the congestion, K5, K6, and K7 are in direction away from the High wall, KW12, KW13 and KW14 in direction up the High wall.

Formatted: Indent: Left: 0.63 cm

Table 10. Maximum overpressure at various probe locations for CASE-E obtained using ~~experiments~~numerical simulations~~.~~.

Sl. No.	Monitoring Location	Maximum overpressure Numerical predictions (barg)
Away from High wall		
1	K1	0.832
2	K2	0.957
3	K3	1.008
4	K4	1.086
5	K5	0.599
6	K6	0.656
7	K7	0.57
On the High wall		

8	KW12	0.844
9	KW13	0.781
10	KW14	0.752

Maximum values of overpressures are extracted at each probe and are tabulated in Table 10. Figure A4 shows the plots of maximum overpressures as a function of distance. The peak overpressure is observed at the K4, which is within the congestion. The ignition in this simulation is close to the High wall, which makes the flame to enter the rig congestion at one end, leading to the flame acceleration in away from the High wall direction. Due to the confinement of the High and low wall, there was buildup of the pressure leading to higher overpressure at KW12 on the High wall. It is worth noting that peak overpressure observed is higher for 3 wall case than for 2 wall and 1 wall, case.

~~Maximum values of overpressures are extracted at each probe and are tabulated in Table 10. Figure A4 shows the plots of maximum overpressures as a function of distance. The peak overpressure is observed at the K4, which is within the congestion. The ignition in this simulation is close to the High wall, which makes the flame to enter the rig congestion at one end, leading to the flame acceleration in away from the High wall direction. Due to the confinement of the High and low wall, there was buildup of the pressure leading to higher overpressure at KW12 on the High wall. It is worth noting that peak overpressure observed is higher for 3 wall case than for 2 wall and 1 wall, case.~~

5.2 Effects of ignition location and number of confining walls on overpressures

The ignition location and number of confining walls to the premixed vapour cloud have significant effect on the overpressure trends.

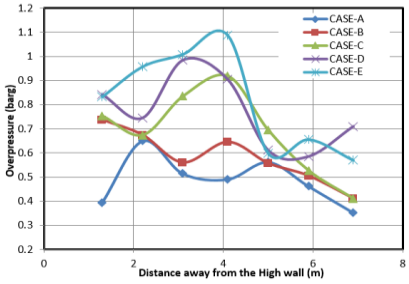

Figure 20. Maximum overpressure obtained using simulations away from High wall. CASE–A: One wall scenario (High wall ignition), CASE–B: Two wall scenario (Low wall ignition) CASE–C: Two wall scenario (High wall ignition), CASE–D: Three wall scenario (Low wall ignition) and CASE–E: Three wall scenario (High wall ignition).

Formatted: Centered

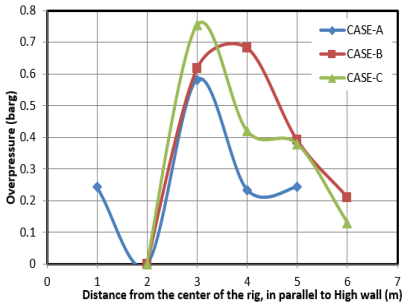

Figure 21. Maximum overpressure obtained using simulations parallel to High wall. CASE–A: One wall scenario (High wall ignition), CASE–B: Two wall scenario (Low wall ignition) CASE–C: Two wall scenario (High wall ignition), CASE–D: Three wall scenario (Low wall ignition) and CASE–E: Three wall scenario (High wall ignition).

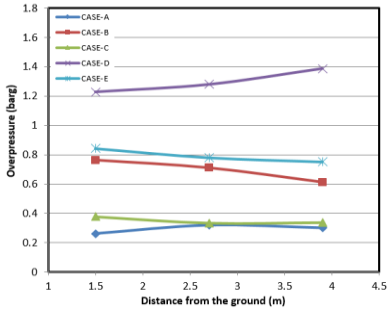

Figure 22. Maximum overpressure obtained using simulations ~~obtained~~ on the High wall. CASE–A: One wall scenario (High wall ignition), CASE–B: Two wall scenario (Low wall ignition), ~~C~~CASE–C: Two wall scenario (High wall ignition), CASE–D: Three wall scenario (Low wall ignition) and CASE–E: Three wall scenario (High wall ignition).

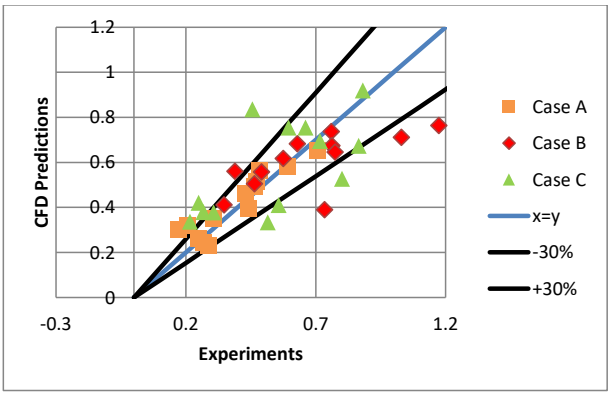

Formatted: Centered

Figure 23. Comparison of maximum overpressure at different probes obtained using experiments and simulations for CASE-A,B and C. Black and blue lines corresponds to ±30 % predictions and x=y. CASE–A: One wall scenario (High wall ignition), CASE–B: Two wall scenario (Low wall ignition), CASE–C: Two wall scenario (High wall ignition).

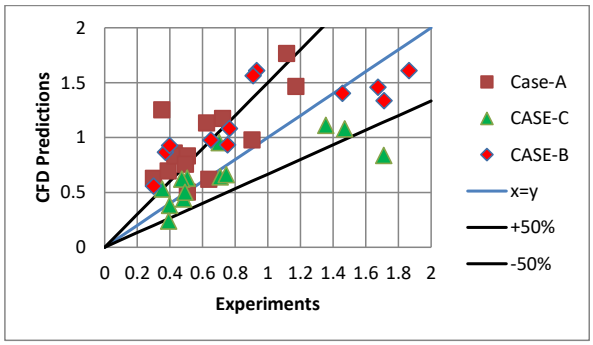

Figure 24. Comparison of positive impulse at different probes obtained using experiments and simulations for CASE-A,B and C. Black and blue lines corresponds to ±30 % predictions and x=y. CASE–A: One wall scenario (High wall ignition), CASE–B: Two wall scenario (Low wall ignition), CASE–C: Two wall scenario (High wall ignition).

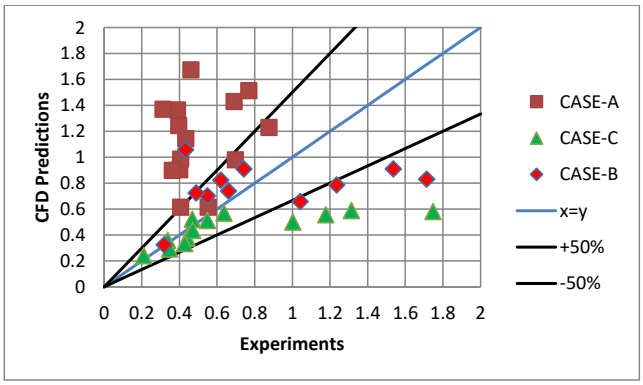

Figure 25. Comparison of absolute values of negative impulse at different probes obtained using experiments and simulations for CASE-~~A,B~~A, B and C. Black and blue lines corresponds to ±30 % predictions and x=y. CASE–A: One wall scenario (High wall ignition), CASE–B: Two wall scenario (Low wall ignition), CASE–C: Two wall scenario (High wall ignition).

In order to better understand effects of ignition location and increase in number of confining walls on overpressure, the results of peak overpressure from CASE-A to CASE-E are compared

in Figs. 20-22. The overpressures have increased in magnitude with an increase in confinement in both away (i.e., from 0.65 bar to 1.1 bar) and parallel to High wall directions (i.e., from 0.58 bar to 0.78 bar). The overpressure increases from 0.3 bar to 0.8 bar on high wall. There is also change in the location of the peak overpressure (from K2 to K4) with the increase in confinements in away from High wall direction. Figure 20 shows that changing the ignition location from low wall to High wall leads to increase the overpressure from 0.75 bar to 0.92 bar in away from high wall location and parallel to High wall directions (i.e., from 0.7 bar to 0.75 bar). However, on high wall the overpressure decreases from 0.7 bar to 0.3 bar, respectively. The peak overpressure location moved away from the High wall (Fig. 20) and in the case of the ignition near the Low wall, the location of peak overpressure is shifting towards the High wall (Fig. 20). In the parallel to High wall direction, the peak overpressure was observed within the congestion for the near high wall ignition, whereas for the near Low wall ignition, peak overpressure location was outside the rig congestion. The peak overpressure location is similar for both the ignition location on the High wall (Fig. 22).

6. Summary and Conclusions

Experimental results and numerical prediction of the overpressure generated in the hydrogen vapor cloud deflagrations for the congestion levels that could be typical of a hydrogen cylinder storage facility are presented and analysed in detail. The worst-case scenario of near stoichiometric hydrogen-air vapor cloud engulfing the hydrogen cylinder storage facility is numerically simulated using OpenFOAM toolbox solver. The flame surface wrinkling model is employed to model the turbulent flame deflagrations. Overall, five scenarios are studied involving a change in number of confining walls from one to three and the ignition location being either near the High or Low wall. The simulation predictions for the three of the cases are compared with experiments. The results demonstrate that the number of confining walls and ignition location affect significantly the combustion process and hence the generated overpressures. The overpressures have increased in magnitude with the increase in confining walls in both away and parallel to High wall directions. There is a clear trend of higher overpressure magnitudes for explosions confined by high wall then by the low wall.

The comparisons between model predictions and experimental data presented in this paper show that a ~~state-of-art~~well ~~-CFD~~validated CFD explosion model can provide reasonably accurate predictions of the development of hydrogen/air explosions in complex geometries. Thus, such models can be used with confidence to explore geometries beyond those tested in experiments, and examine layouts that might mitigate consequences in the albeit unlikely event of hydrogen leakage, ignition, and explosion. The experimental knowledge gap can be supplemented by the numerical predictions.

Acknowledgements

The authors thank Shell Alternate Energies – Hydrogen for permission to publish this paper.

REFERENCES

1. L. C. Shirvill, T. A. Roberts, M. Royle, D. B. Willoughby and P. Sathiah, Effects of congestion and confining walls on turbulent deflagrations in a hydrogen storage

Facility-Part 1: Experimental Study. Accepted for publication in International Journal of Hydrogen Energy.
2. Tabor, G. and H.G. Weller, Large Eddy Simulation of Premixed Turbulent Combustion Using Ξ Flame Surface Wrinkling Model. Flow, Turbulence and Combustion, 2004. **72**(1): p. 1-27.
3. V. C. Madhav Rao, J. Wen, and V.H.Y. Tam. Numerical Study of Hydrogen Explosions in a Vehicle Refill Environment. in 3rd International Conference on Hydrogen Safety. 2009. Corsica, France
4. Shirvill LC, Roberts TA. Designing for safe operations: Understanding the hazards posed by high-pressure leaks from hydrogen refuelling systems. In: USA National Hydrogen Association annual hydrogen conference, March 12-16, 2006, Long Beach, California, USA.
5. Shirvill, L.C., et al., Safety studies on high-pressure hydrogen vehicle refuelling stations: Releases into a simulated high-pressure dispensing area. International Journal of Hydrogen Energy, 2012. **37**(8): p. 6949-6964.
6. Takeno, K., et al., Dispersion and explosion field tests for 40 MPa pressurized hydrogen. International Journal of Hydrogen Energy, 2007. **32**(13): p. 2144-2153.
7. Tanaka, T., et al., Experimental study on hydrogen explosions in a full-scale hydrogen filling station model. International Journal of Hydrogen Energy, 2007. 32(13): p. 2162-2170.
8. V.L. Zimont, Gas premixed combustion at high turbulence. Turbulent flame closure combustion model, Experimental Thermal and Fluid Science, Volume 21, Issue 1, 2000, Pages 179-186.
9. Baraldi, D., et al., Numerical analysis of release, dispersion and combustion of liquid hydrogen in a mock-up hydrogen refuelling station. Journal of Loss Prevention in the Process Industries, 2009. **22**(3): p. 303-315.
10. Makarov, D., et al., An inter-comparison exercise on CFD model capabilities to predict a hydrogen explosion in a simulated vehicle refuelling environment. International Journal of Hydrogen Energy, 2009. 34(6): p. 2800-2814.
11. Wen, J.X., V.C. Madhav Rao, and V.H.Y. Tam, Numerical study of hydrogen explosions in a refuelling environment and in a model storage room. International Journal of Hydrogen Energy, 2010. 35(1): p. 385-394.
12. Pope, S.B., Turbulent Flows. 2000: Cambridge University Press.
13. OpenFOAM Ltd.; Available from: http://www.openfoam.com/.
14. Weller, H.G., et al., Application of a flame-wrinkling les combustion model to a turbulent mixing layer. Symposium (International) on Combustion, 1998. **27**(1): p. 899-907.
15. Fureby, C., et al., A comparative study of subgrid scale models in homogeneous isotropic turbulence. Physics of Fluids, 1997. **9**(5): p. 1416-1429.
16. Gülder, Ö.L., Turbulent premixed flame propagation models for different combustion regimes. Symposium (International) on Combustion, 1991. **23**(1): p. 743-750.
17. Metghalchi, M. and J.C. Keck, Burning velocities of mixtures of air with methanol, isooctane, and indolene at high pressure and temperature. Combustion and Flame, 1982. 48: p. 191-210.
18. Dahoe, A.E., Laminar burning velocities of hydrogen–air mixtures from closed vessel gas explosions. Journal of Loss Prevention in the Process Industries, 2005. 18(3): p. 152-166.

7. Appendix 1: Additional results for CASE-A, B, C, D and E.

The overpressure trends are plots w.r.t the high wall along with available experimental results for the five numerical cases considered in the present study.

~~Figure A1 shows comparison of maximum overpressure function of distance at different probes a) away from High wall, b) parallel to High wall and c) on High walls for CASE-A.~~

Formatted: Font: (Default) Times New Roman, 12 pt

Formatted: Left, Space After: 10 pt, Line spacing: Multiple 1.15 li

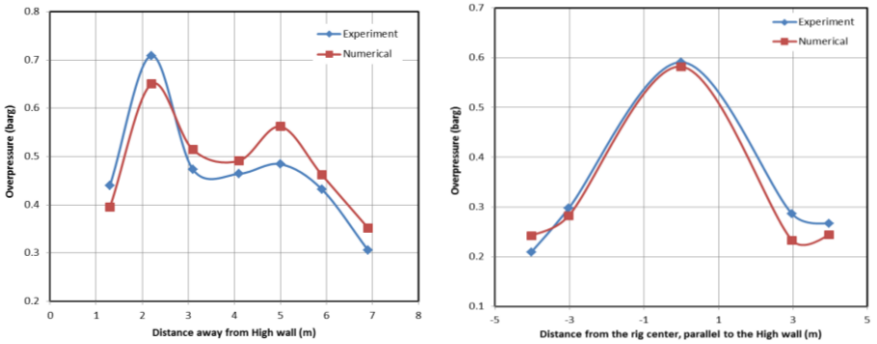

(a)

(b)

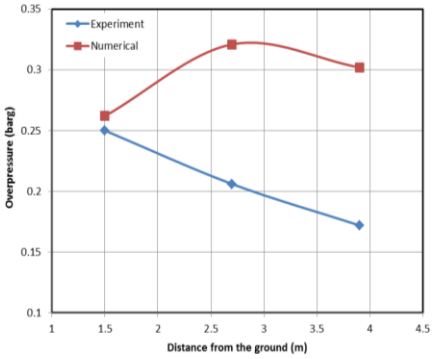

(c)

Figure A1. Comparison of maximum overpressure in CASE-A as a function of distance at different probes a) away from High wall, b) parallel to High wall and c) on High walls.

~~Figure A2 shows comparison of maximum overpressure function of distance at different probes a) away from High wall, b) parallel to High wall and c) on High walls for CASE-B.~~

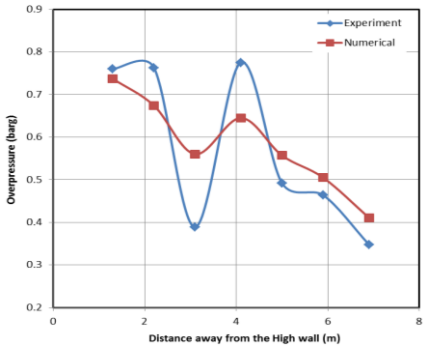

(a)

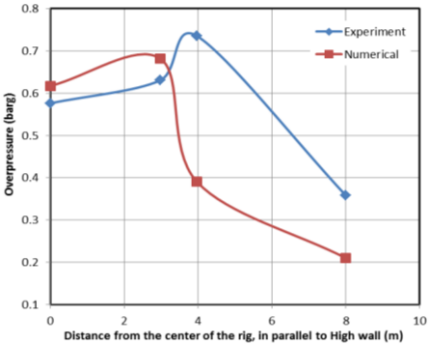

(b)

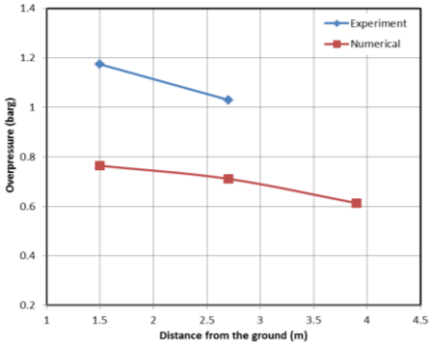

(c)

Figure A2. Maximum overpressure measured in CASE-B at different probes a) away from High wall, b) parallel to High wall and c) on High walls.

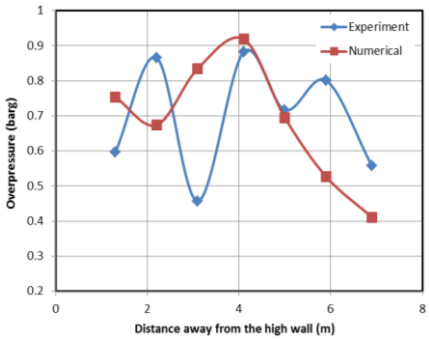

(a)

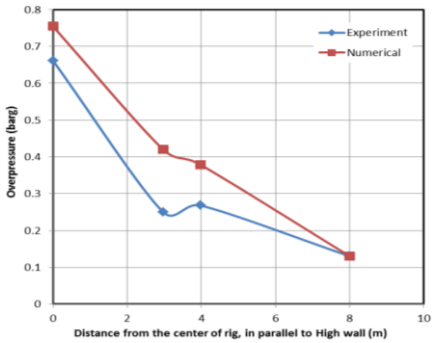

(b)

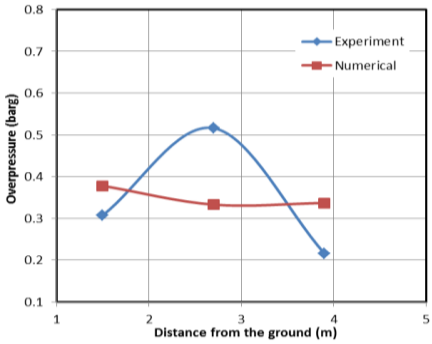

(c)

Figure A3. Profiles of maximum overpressure measured in CASE-C as a function of distance at different probes a) away from High wall, b) parallel to High wall and c) on High walls

~~Figure A3 shows comparison of maximum overpressure function of distance at different probes a) away from High wall, b) parallel to High wall and c) on High walls for CASE–C.~~

~~Figure A4 shows comparison of maximum overpressure function of distance at different probes a) away from High wall, b) parallel to High wall and c) on High walls for CASE-D.~~

~~Figure A5 shows comparison of maximum overpressure function of distance at different probes a) away from High wall, b) parallel to High wall and c) on High walls for CASE-E.~~

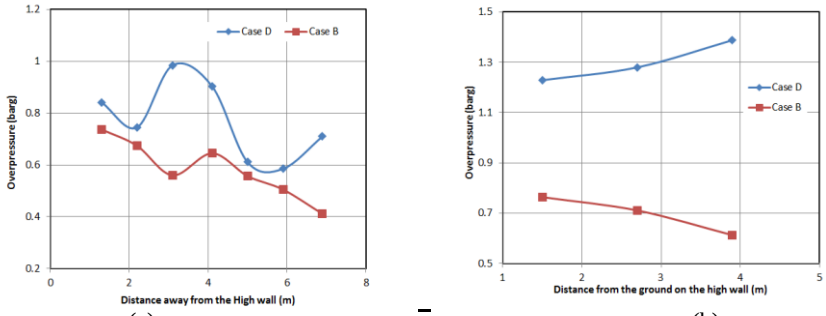

(a) (b)

Figure A4. Maximum overpressure obtained ~~using~~ in numerical simulations in CASE-D & B for low wall ignition as a function of distance at different probes a) away from High wall and b) on High wall.

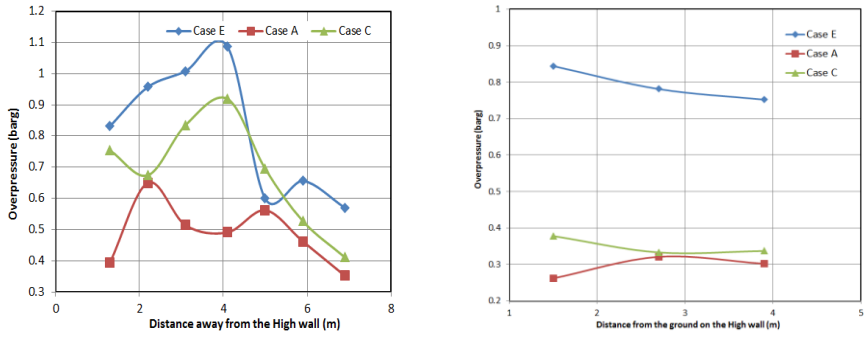

(a) (b)

Figure A5. Maximum overpressure obtained ~~using~~ in numerical simulations in CASE A, C & E for high wall ignition as a function of distance at different probes a) away from High wall and b) on High wall.